T.R.
GEBZE TECHNICAL UNIVERSITY
GRADUATE SCHOOL

OPTIMIZATION OF POWER OUTPUT IN SMART COMPOSITE PANEL INTEGRATED WITH PIEZOELECTRIC PATCHES

MUSTAFA KEMAL ACAR

A THESIS OF MASTER OF SCIENCE
DEPARTMENT OF MECHANICAL ENGINEERING

ADVISOR: ASSIST. PROF. PEYMAN LAHE MOTLAGH

DECEMBER 2023

T.R.

GEBZE TECHNICAL UNIVERSITY

GRADUATE SCHOOL

OPTIMIZATION OF POWER OUTPUT IN SMART COMPOSITE PANEL INTEGRATED WITH PIEZOELECTRIC PATCHES

MUSTAFA KEMAL ACAR

A THESIS OF MASTER OF SCIENCE

DEPARTMENT OF MECHANICAL ENGINEERING

ADVISOR: ASSIST. PROF. PEYMAN LAHE MOTLAGH

DECEMBER 2023

T.C.
GEBZE TEKNİK ÜNİVERSİTESİ
LİSANSÜSTÜ EĞİTİM ENSTİTÜSÜ

PİEZOELEKTRİK YAMALARLA ENTEGRE EDİLMİŞ AKILLI KOMPOZİT PANELDE GÜÇ ÇIKTISININ OPTİMİZASYONU

MUSTAFA KEMAL ACAR

YÜKSEK LİSANS TEZİ
MAKİNE MÜHENDİSLİĞİ ANABİLİM DALI

DANIŞMAN: DR.ÖĞR. ÜYESİ PEYMAN LAHE MOTLAGH

ARALIK 2023

GEBZE TEKNİK ÜNİVERSİTESİ	**M.Sc. JURY APPROVAL FORM**

A Thesis/Dissertation submitted by **Mustafa Kemal Acar,** whose thesis defense exam was made on 13/12/2023 by the jury formed with the 27/11/2023 date and 2023/21 numbered decision of the GTU Graduate Administrative Board, was accepted as a **MASTER of SCIENCE** thesis in the **Department of Mechanical Engineering.**

JURY

JURY MEMBERS

(THESIS ADVISOR): ASSISTANT PROFESSOR PEYMAN LAHE MOTLAGH

MEMBER : ASSOCIATE PROFESSOR BEKİR BEDİZ

MEMBER : ASSISTANT PROFESSOR RECEP ÖNLER

APPROVAL

Gebze Technical University Graduate Administrative Board

…..…/…..…/..…… date and ……/…….. numbered decision.

SIGNATURE/MÜHÜR

Dedication / İthaf

To my
Family and my
Lovely Wife

ABSTRACT

This research introduces an innovative approach to explore energy generation in intelligent structures, employing composite panels integrated with piezoelectric patches. The investigation revolves around the dynamics of symmetry-balanced laminated composites, examining natural frequency and mode shapes through modal and harmonic analysis, utilizing the Rayleigh-Ritz Method. To compute the kinetic and potential energy components of the piezoelectric patches at a local level, piecewise Heaviside functions are applied. Subsequently, these energy components are integrated into the equations of motion alongside those of the host composite plate. By subjecting the laminated composite with piezoelectric patches to forced vibration while varying the lamination parameters, the power output is optimized. The findings highlight the significant influence of the lamination parameter on the power output, demonstrating that modifying it can lead to enhancements. The proposed framework holds great potential in the efficient design and optimization of composite panels with integrated piezoelectric patches, benefiting energy harvesting applications. Furthermore, it enables the exploration of the dynamics of other intelligent structures that incorporate piezoelectric elements.

Keywords: Composite panel, Energy harvesting, Optimization, Piezoelectric patches, Rayleigh-Ritz method.

ÖZET

Araştırma kapsamında, piezoelektrik yamalar ile entegre edilmiş kompozit paneller kullanılarak akıllı yapılardaki enerji üretimini keşfetmek için yenilikçi bir yaklaşım sunulmaktadır. Bu araştırma, simetrik olarak dengeli lamine kompozitlerin dinamikleri etrafında dönmekte ve Rayleigh-Ritz Yöntemi kullanılarak modal ve harmonik analiz yoluyla doğal frekans ve mod şekillerini incelemektedir. Piezoelektrik yamaların kinetik ve potansiyel enerji bileşenlerini yerel düzeyde hesaplamak için parçalı Heaviside fonksiyonları uygulanmıştır. Daha sonra, bu enerji bileşenleri ana kompozit plakanınkilerle birlikte hareket denklemlerine entegre edilmiştir. Piezoelektrik yamalar ile entegre edilmiş lamine kompozit malzemenin laminasyon parametreleri değiştirilirken zorlanmış titreşime maruz bırakılarak güç çıkışı optimize edilmiştir. Bulgular, laminasyon parametrelerinin güç çıkışı üzerindeki önemli etkisini vurgulamakta ve bunun değiştirilmesinin iyileştirmelere yol açabileceğini göstermektedir. Önerilen çerçeve, piezoelektrik yamalara sahip kompozit panellerin verimli tasarımı ve optimizasyonunda büyük bir potansiyele sahiptir ve enerji eldesinde fayda sağlar. Ayrıca, piezoelektrik elemanlar içeren diğer akıllı yapıların dinamiklerinin keşfedilmesine de olanak sağlamaktadır.

Anahtar Kelimeler: Enerji eldesi, Kompozit panel, Optimizasyon, Piezoelektrik yamalar, Rayleigh-Ritz yöntemi.

ACKNOWLEDGEMENTS

I would like to express my deep and sincere gratitude to my supervisor, Asst. Dr. Peyman Lahe MOTLAGH, who not only shared his profound scientific knowledge with me but also taught me great lessons of life. His support, suggestions and encouragement gave me the drive and will to complete this work.

Finally, I am grateful to my parents and my wife for their love and support.

TABLE OF CONTENTS

LIST OF SYMBOLS AND ABBREVIATIONS

a	:	Lenght of plate
b	:	Width of plate
h_s	:	Thickness of plate
l_p	:	Length of patch
w_p	:	Width of patch
h_p	:	Thickness of patch
R_l	:	Resistive load
γ_{zx}	:	Transverse shear strains
γ_{yz}	:	Transverse shear strains
ε_{zz}	:	Normal strain
σ_{zz}	:	Normal stress
Y_s	:	Young's modulus
v_s		Poisson's ratio
$\{N\}$	:	Stress resultants
$\{M\}$	:	Moment resultants
K	:	Panel curvatures
A	:	Tensor of in-plane stiffness
B	:	Tensor of in-plane/bending coupling
D	:	Tensor of bending stiffness
V_1	:	The normalized lamination parameter
V_3	:	The normalized lamination parameter
N_l	:	The number of layers in the laminate
t_k	:	The thicknesses of individual layers
θ_k	:	The angles of each layer
U	:	The material invariants
e_{31}	:	Piezoelectric constant
$\bar{\varepsilon}_{33}^{T}$	:	Dielectric permittivity at constant stress
$\bar{\varepsilon}_{33}^{S}$	:	Dielectric permittivity at constant strain
$v_i(t)$	:	Electrical potential difference
E_{33}	:	Electric field
D_3	:	Electric displacement field
c_{ij}	:	Reduced modulus of elasticity
δ	:	Variation
KE	:	Kinetic energy
PE	:	Potential energy
W_p	:	Work done by non-conservative forces
S	:	Surface area of the system
$m(x,y)$	:	Mass
$\bar{w}$	:	Velocity
ρ_s	:	Density of the thin composite plate
ρ_p	:	Density of the thin composite plate
$P(x,y)$	:	Indicator function

H	:	Heaviside unit step function
Vs	:	Volumes of composite plate
V_p	:	Volumes of piezoelectric patch
S_s	:	Surface area of a composite plate
D_{ij}	:	Bending stiffness matrix
Q_{ij}	:	Reduced stiffness matrix
S_p	:	Surface area of the piezoelectric patches
$v(t)$	:	Voltage
$f(t)$	:	Amplitude of the force
$\delta(x)$	:	Dirac delta functions along the x axis
w	:	Displacement of the system
$\mu_{ij}(t)$	:	Generalized modal coordinates
N	:	Vibration modes in the y coordinates
R	:	Vibration modes in the x coordinates
$U_{ij}W_{ij}(x,y)$	:	Assumed modes
U_{ij}	:	Rayleigh's quotient
$W_{ij}(x,y)$	:	Trial functions
$k(x)$	:	Weighting function
$\phi_1(x)$	:	Orthogonal polynomials
$K_{ij,kl}$	:	Stiffness term
$M_{ij,kl}$	:	Mass term
$i_l^{\mathrm{p}}(t)$	:	Current source
$(C_p)_l$	:	Equivalent capacitance
θ_l	:	Electromechanical coupling term
ω_{rs}	:	Natural frequency
ζ_{rs}	:	Modal damping ratio
H_{rs}	:	Complex amplitude of the modal response
λ	:	Eigenvalues
C_{pc}	:	Capacitance
w_1	:	First natural frequency
G_{12}	:	Shear elastic modulus
Ω	:	Ohm
Cs_{mnij}	:	Stiffness term of the host structure
Cp_{mnij}	:	Stiffness term of the piezo patch

LIST OF FIGURES

LIST OF TABLES

1. INTRODUCTION

Over the past few years, the global quest for efficient and eco-friendly energy harvesting solutions has been on the rise to cater to the escalating energy demands of our modern world. Amidst a range of techniques, one particularly promising method involves incorporating piezoelectric materials into composite structures(Detwiler et al., 1995). This integration has demonstrated remarkable potential in transforming ambient mechanical vibrations into practical electrical energy. By embracing this approach, the development of intelligent materials becomes possible, empowering them to function as self-powered sensing systems, wireless sensor networks, and various energy-autonomous devices(Wan et al., 2023).

The study utilized laminated composites, which are materials composed of multiple layers or plies bonded together to form a single, cohesive structure. These layers, referred to as laminae, are typically made from diverse materials like fibers, fabrics, films, or sheets, held together by an adhesive or resin. Figure 1.1 shows a laminated composite consisting of matrix, fibers, and laminates(Khetre et al., n.d.).

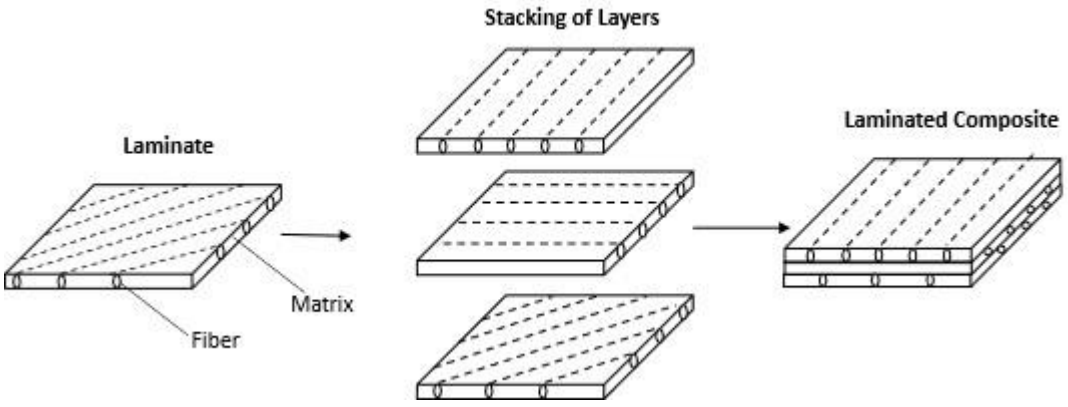

Figure 1.1: Laminated composite.

The main purpose of employing laminated composites is to combine the favorable properties of different materials, resulting in a composite material with enhanced

overall performance. Each layer in the laminate contributes specific characteristics, such as high strength, stiffness, impact resistance, or thermal stability, depending on the materials employed. Engineers can strategically arrange and bond these layers to customize the properties of the laminated composite according to specific application requirements. One significant advantage of laminated composites lies in their ability to offer considerable strength and stiffness while keeping the weight relatively low. This aspect is particularly crucial in industries like aerospace, automotive, and sports equipment manufacturing, where lightweight materials play a vital role in achieving fuel efficiency, performance, and durability(Park et al., 2001).

However, despite the numerous advantages of composite laminates, they also face a significant challenge posed by excessive vibrations, which can lead to mechanical failures and reduce the overall lifespan of the material (Fleming & Moheimani, 2003). Nevertheless, it is essential to acknowledge that these vibrations can be harnessed to generate energy. Vibration energy harvesting involves the process of capturing and converting mechanical vibrations into usable electrical energy. Various methods and technologies exist for harvesting energy from vibrations, tailored to specific applications and requirements. These techniques encompass piezoelectric (Kim et al., 2011), electromagnetic (Yang et al., 2009), and electrostatic transduction mechanisms (Torres & Rincon-Mora, 2009), which are commonly employed for vibration energy harvesting. Among these, piezoelectric energy harvesting stands out as a preferred choice for several reasons:

Piezoelectric materials outperform electromagnetic and electrostatic methods in terms of power density, meaning they can generate more electrical power from a given input of mechanical vibration energy. This higher power density enables more efficient energy conversion and better utilization of available vibration energy. One key advantage of piezoelectric energy harvesting is its direct conversion of mechanical vibrations into electrical energy, eliminating the need for complex additional mechanisms or components(Sezer & Koç, 2021). This simplicity leads to a more straightforward and efficient energy harvesting system.

Moreover, piezoelectric materials exhibit a wide frequency response range, making them capable of harvesting energy from a broader spectrum of vibrations. This

flexibility in frequency response makes them suitable for capturing energy from various sources, encompassing both low-frequency ambient vibrations and high-frequency mechanical vibrations(Covaci & Gontean, 2020).

In terms of manufacturing, piezoelectric energy harvesters have an advantage over their electromagnetic and electrostatic counterparts. Piezoelectric materials, such as ceramics or polymers, can be easily integrated into devices or structures, streamlining the manufacturing process, and reducing costs.

Furthermore, piezoelectric energy harvesters can be designed to be compact and lightweight, which is particularly beneficial for applications where size and weight constraints are crucial, such as wearable devices or portable electronics. Their small form factor allows for easy integration into various systems without adding significant bulk or weight(Priya et al., 2019).

Another notable aspect of piezoelectric materials is their durability and robustness, making them well-suited for long-term and reliable operation even in harsh environmental conditions. They can withstand mechanical stresses, temperature variations, and other challenging operating conditions, ensuring the energy harvesting system's longevity and stable performance over time(Ghazanfarian et al., 2021).

These materials have received considerable attention and widespread adoption in diverse applications, such as structural health monitoring, energy harvesting, and shunt damping.

Structural Health Monitoring (SHM) is a critical application of piezoelectric materials. SHM is the process of continuously and remotely monitoring the condition and performance of structures, such as bridges, buildings, aircraft, pipelines, and more. The goal of SHM is to detect any structural damage, deterioration, or anomalies early on, allowing for timely maintenance and preventing potential failures. Piezoelectric materials are integral to SHM due to their ability to sense and transmit mechanical vibrations and stress into electrical signals. Here's how SHM works and how piezoelectric materials are used in this context (Ju et al., 2023):

Installation of Piezoelectric Sensors: Piezoelectric sensors or patches are strategically placed on or within the structure being monitored. These sensors are typically bonded to the surface or embedded in the structure at key locations susceptible to stress, strain, or potential damage.

Vibration and Stress Sensing: When the monitored structure is subjected to mechanical loads, vibrations, or stress, these piezoelectric sensors respond by generating electrical signals. The amplitude and frequency of these signals are directly related to the mechanical forces experienced by the structure.

Data Acquisition: The electrical signals generated by the piezoelectric sensors are collected by data acquisition systems. These systems may include analog-to-digital converters (ADCs) to convert the analog signals into digital data for further analysis.

Data Analysis: The collected data is processed and analyzed using various algorithms and techniques. Any deviations from the expected signal patterns are indicators of structural anomalies, damage, or fatigue. Advanced signal processing methods are employed to distinguish between normal variations and potential issues.

Damage Detection and Assessment: SHM systems continuously monitor the structural integrity of the system in real-time or periodically. By comparing current data to baseline measurements, they can detect and locate structural damage, including cracks, delamination, corrosion, and fatigue. The severity of damage can also be assessed based on the changes in the electrical signals.

Alerts and Maintenance: When SHM systems detect significant deviations from the baseline or predefined thresholds, they can trigger alerts or notifications to maintenance personnel. This allows for timely inspection, maintenance, or repair, helping to prevent catastrophic failures and ensure the long-term reliability of the structure.

Long-Term Monitoring: SHM systems using piezoelectric materials offer the advantage of continuous, long-term monitoring. This allows for the early detection of

damage that may not be apparent during visual inspections, and it provides valuable data for assessing the structure's health over time.

Cost Savings and Safety: SHM helps reduce maintenance costs by allowing targeted repairs and replacements rather than routine, time-based maintenance. It also enhances safety by preventing unexpected structural failures in critical infrastructure.

In summary, Structural Health Monitoring leverages piezoelectric materials to continuously monitor the condition of structures, detect damage or anomalies early, and enable data-driven maintenance decisions. This technology contributes to the safety, reliability, and cost-efficiency of various types of infrastructure and mechanical systems.

This particular use has been extensively investigated and analyzed in academic literature: (Qing et al., 2019) and (Duan et al., 2010) have delved into the exploration of structural health monitoring, focusing on the application of piezoelectric materials. Through their research, they have investigated the integration of piezoelectric elements into structures, allowing these materials to function as sensors for monitoring structural health and integrity.

Piezoelectric shunt damping is accomplished by adding an electrical shunt circuit containing piezoelectric materials to the vibrating system. It is given Figure 1.2. These mechanisms shunt a connected piezoelectric transducer with electrical impedance to reduce structural vibration. Propagation is by means of joule heating through the resistor R. Here's a more detailed explanation of shunt damping(Yan et al., 2017):

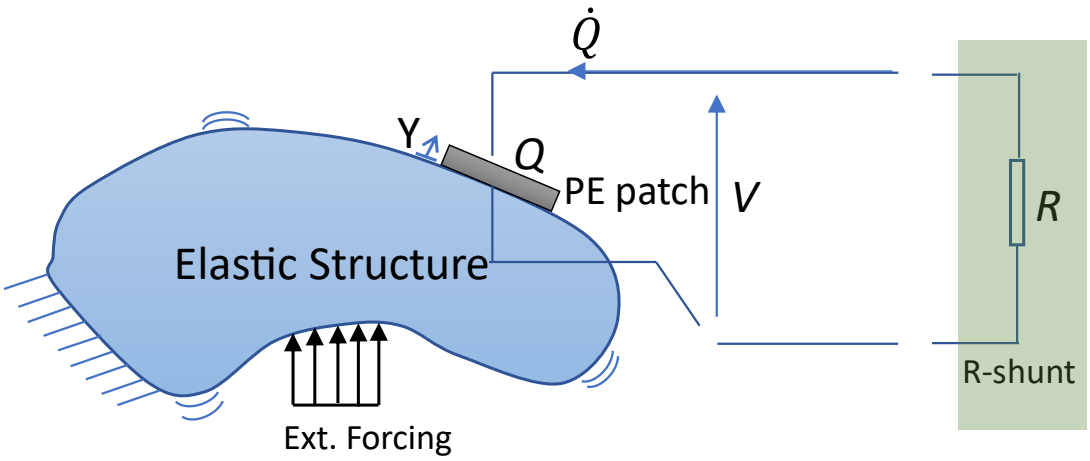

Figure 1.2: Piezoelectric shunt damping.

Vibration in Mechanical Systems: Mechanical systems, such as bridges, buildings, machinery, and aerospace structures, often experience vibrations. These vibrations can occur due to various reasons, including external forces, resonance, and operational loads. Uncontrolled vibrations can lead to performance issues, discomfort, and even structural damage.

Piezoelectric Shunt Circuit: Shunt damping introduces a piezoelectric shunt circuit into the vibrating system. This circuit typically includes a piezoelectric actuator (a piezoelectric material) and associated electrical components.

Piezoelectric Actuator: The piezoelectric actuator is a key component of the shunt circuit. When an electrical voltage is applied to the piezoelectric actuator, it experiences a mechanical deformation or motion. This deformation is a result of the piezoelectric effect, where certain materials generate mechanical displacement when subjected to an electrical field.

Dissipation of Mechanical Energy: In shunt damping, the piezoelectric actuator is strategically placed at or near the location where vibrations are a concern. When the mechanical structure vibrates, it generates mechanical energy. The electrical shunt circuit is designed to apply a voltage to the piezoelectric actuator that is out of phase with the mechanical motion. This means that when the structure is moving in one

direction, the piezoelectric actuator moves in the opposite direction due to the applied voltage.

Energy Dissipation: As the piezoelectric actuator moves in response to the vibrations, it consumes electrical energy. This energy consumption is effectively a conversion of mechanical energy into electrical energy. The dissipation of energy in this manner results in the reduction of vibration amplitudes in the mechanical structure.

Vibration Control and Damping: By dissipating mechanical energy through the piezoelectric shunt circuit, shunt damping can effectively control and reduce vibrations. It is particularly useful for mitigating resonance and reducing the impact of external forces on structures.

Advantages of Shunt Damping:

Shunt damping offers several advantages, including:

Improved system stability and performance by reducing vibrations.

Enhanced structural integrity and longevity by reducing fatigue-related damage.

Greater comfort for occupants in vibrating environments.

Precision control over damping levels.

Applications: Shunt damping can be applied to various systems, including civil infrastructure like bridges and buildings, aerospace structures, industrial machinery, and more. It is especially valuable in situations where precise control over vibration levels is critical.

In summary, shunt damping is a technique that uses piezoelectric materials to dissipate mechanical energy and reduce vibrations in mechanical systems and structures. It is an effective method for enhancing performance, safety, and comfort in a wide range of applications.

The works of (Han et al., 2013) and (Lahe et al., 2018) have contributed to the increasing prominence of shunt damping, focusing on the application of piezoelectric materials for this purpose. According to these studies, vibration amplitudes can be reduced, and the damping characteristics of the system can be improved.

Energy harvesting via piezoelectric materials is a technology that captures and converts mechanical vibrations or strain energy into electrical energy using piezoelectric materials. A typical piezoelectric energy harvesting system in Figure 1.3.

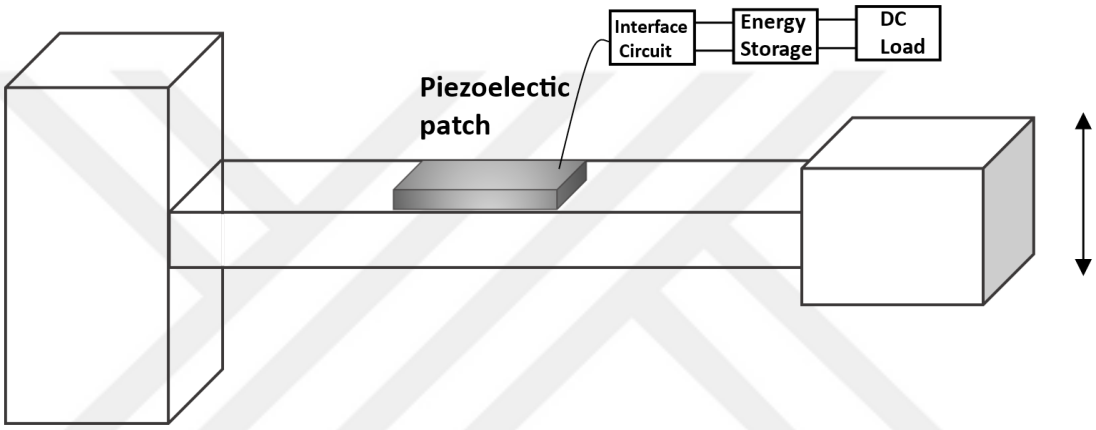

Figure 1.3: An example of a piezoelectric energy harvesting system.

These materials have a unique property called the piezoelectric effect, which allows them to generate an electrical voltage when subjected to mechanical stress or vibrations and vice versa. Here's a detailed explanation of energy harvesting via piezoelectric materials(Li & Lee, 2022):

Energy Source: The energy source for piezoelectric energy harvesting is mechanical vibrations or strain in the environment. These vibrations can originate from various sources, such as: Vibrations from machinery and equipment, oscillations caused by wind or water currents, structural vibrations in buildings or bridges.

Piezoelectric Generators: Piezoelectric energy harvesting systems typically consist of piezoelectric generators or transducers. These generators are designed to capture

mechanical vibrations and convert them into electrical energy. The key components include:

Mechanical Coupling: To maximize energy capture, the piezoelectric material is mechanically coupled to the source of vibrations. This ensures that the mechanical motion of the source is efficiently transferred to the piezoelectric material.

Electrical Circuit: The generated electrical energy is collected and processed through an electrical circuit. This circuit may include rectifiers to convert the generated alternating current (AC) voltage into direct current (DC) voltage, energy storage elements (e.g., capacitors or batteries) for storing the harvested energy, and power management electronics to regulate the output voltage and current.

Conversion of Mechanical to Electrical Energy: When the piezoelectric material is subjected to mechanical vibrations or stress, it generates electrical voltage and current. The magnitude of the generated electrical energy depends on factors such as the intensity of the vibrations, the properties of the piezoelectric material, and the design of the generator.

Applications: Energy harvesting via piezoelectric materials has a wide range of applications, including:

Wireless Sensors: Powering remote sensors and sensor networks for applications like environmental monitoring, smart agriculture, and industrial automation.

Wearable Electronics: Charging or supplementing the power supply of wearable devices such as fitness trackers, smartwatches, and medical implants with energy generated from body movements.

Internet of Things (IoT): Extending the battery life or enabling battery-free operation of IoT devices, such as smart home sensors and connected devices.

Advantages:

Sustainability: Energy harvesting via piezoelectric materials is a sustainable technology that harnesses ambient mechanical energy, reducing the need for traditional power sources.

Extended Battery Life: In many applications, it can significantly extend the lifespan of batteries or eliminate the need for them altogether.

Maintenance-Free: Devices powered by piezoelectric energy harvesting can operate for extended periods without the need for frequent battery replacements or maintenance.

In summary, energy harvesting via piezoelectric materials is a technology that leverages the piezoelectric effect to capture mechanical vibrations and convert them into electrical energy. This technology has a wide range of practical applications and offers sustainability, efficiency, and the potential for longer-lasting and maintenance-free devices.

The research about the energy harvesting conducted by (Gozum et al., 2018) and (Aridogan et al., 2014) has primarily focused on energy harvesting, highlighting the promising potential of piezoelectric materials in this area.

The effectiveness of piezoelectric energy harvesting systems depends on several critical factors that significantly influence their overall efficiency. Firstly, the size and shape of the piezoelectric material used in the system play a pivotal role in determining its energy harvesting capabilities. The geometric characteristics of the piezoelectric material can be carefully designed to optimize its electrical properties and enhance the energy conversion process. Additionally, the frequency and amplitude of the mechanical vibrations directly impact the magnitude and quality of the electrical energy output. A comprehensive understanding of the intricate interplay between these vibrational parameters and the resulting energy harvesting performance is crucial for developing effective optimization strategies.

Piezoelectric materials, often used as patches or layers, find widespread application in structural engineering, where they are integrated onto the surfaces of flexible beam or

plate-like structures (Motlagh et al., 2021). The focus of this research lies in exploring energy harvesting methods by integrating vibrating laminated composite plates with piezoelectric patches. By incorporating piezoelectric patches into the laminated composite structure, it becomes feasible to harness electrical energy from mechanical vibrations and deformations induced by external forces or ambient sources.

The existing literature contains valuable contributions from researchers regarding the modeling of structures integrated with piezoelectric materials. Initially, (Erturk & Inman, 2009), introduced a lumped parameter model to describe beam-like structures featuring a complete piezoelectric layer. Building on this foundation (Yoon et al., 2016), developed an analytical model for plate-like structures that incorporated a piezoelectric patch, with adaptability for partially covered panels. Taking these advancements further, (Gozum et al., 2018) expanded the scope by creating a model that considered laminated composite panels. Additionally, (Zhou et al., 2018) directed their attention towards smart composite modeling, presenting a fresh and innovative approach to analyzing the vibration behavior of a composite pipe-shaped structure integrated with piezoelectric materials.

Nevertheless, attaining optimal energy harvesting performance necessitates the maximization of power output from the laminated composite integrated with piezoelectric patches. The process of power optimization plays a critical role in enhancing the efficiency and feasibility of energy harvesting systems, as it directly impacts the quantity of electrical energy that can be generated and effectively utilized.

An encouraging approach to boost power output involves adjusting lamination parameters within the composite structure. These parameters encompass elements like stacking sequence, fiber orientations, and layer thicknesses, which collectively govern the mechanical and electromechanical characteristics of the laminated composite. Through careful and deliberate optimization of these parameters, it becomes feasible to customize the structural response and improve the efficiency of electromechanical coupling, ultimately leading to the maximization of power output.

The pursuit of maximizing power output in laminated composites integrated with piezoelectric patches through lamination parameters is a challenging and multifaceted

area of research. It demands a thorough comprehension of how mechanical and electrical properties interact and how various lamination configurations influence the overall performance of the system. As a result, this subject has drawn significant interest from scholars in the smart materials and energy harvesting domain.

Various researchers have utilized the lamination parameters technique as a concise representation of laminated composites' stiffness characteristics, independent of the number of layers and their individual thicknesses. For instance, (Abdalla et al., 2007) utilized lamination parameters to express the fundamental natural frequency of symmetrically laminated panels. Similarly, (Trias et al., 2016) used lamination parameters to determine the optimal stacking sequence that maximizes the fundamental frequency. Moreover, (Honda et al., 2009) optimized lamination parameters to adjust the natural frequencies of laminates based on three performance metrics. Additionally, (Bardell et al., 1997) conducted a vibration analysis of thin, laminated, cylindrically singly-curved shell panels using the finite element method, while (Assaee & Hasani, 2015) investigated the forced vibration response of curved composite cylindrical shells using the spline finite strip method. These research efforts demonstrate the broad application of lamination parameters in analyzing and optimizing the behavior of laminated composites in various structural configurations.

In the existing literature, several methods have been proposed for modeling piezoelectric laminated composite plates. One commonly used approach is Classical Plate Theory (CPT), a two-dimensional mathematical model specifically designed for analyzing thin plates with small deformations. CPT assumes that the plate is thin and uniformly thick, neglecting deformations in the thickness direction compared to those in the plate's plane. Although CPT has certain limitations, such as its inability to accurately model large deformations and shear effects, it remains widely used for modeling straight panels. Researchers have devised various CPT-based models to study the vibration characteristics of piezoelectric layers within laminated composites.

Improving the effectiveness and dependability of piezoelectric energy harvesting systems remains an ongoing endeavor. Despite the potential benefits, the energy generated from smart composites has not received sufficient focus in previous research. In light of this, the current study introduces a novel approach aimed at

optimizing the power output of a smart panel integrated with piezoelectric patches. The proposed method involves selecting an appropriate lamination parameter for the panel, which determines the stacking sequence of its various layers. This lamination parameter plays a pivotal role in influencing the piezoelectric effect and, consequently, the overall energy harvesting performance.

To achieve optimal lamination parameters for a particular application, a blend of numerical modeling techniques can be utilized. Finite Element Analysis (FEA) is a method that can effectively simulate the behavior of the panel, shedding light on how different lamination parameters affect energy harvesting performance. By employing FEA, it becomes possible to compute displacement, strain, and electric potential, thereby gaining a comprehensive understanding of the panel's electromechanical behavior. Furthermore, FEA enables the assessment of the panel's performance under diverse loading conditions, encompassing both static and dynamic loads.

Modal and harmonic analysis are essential for determining the natural frequencies and corresponding mode shapes of smart composites. To achieve these goals, researchers commonly rely on the Rayleigh-Ritz Method, a widely used numerical approach. In this study, the Rayleigh-Ritz Method is employed to calculate the natural frequencies and mode shapes of a smart composite panel integrated with piezoelectric patches.

The analytical model adopted in this research accounts for the geometric discontinuities of the piezoelectric patches and employs piecewise Heaviside functions to derive the kinetic and potential energy components locally. These components are then combined with those of the host composite plate to establish the equations of motion. By using this method, the study gains valuable insights into the dynamic behavior of the smart composite panel and its piezoelectric elements.

Moreover, Hamilton's principle is employed to derive the governing equation of motion. To validate the accuracy and reliability of the analytical model, the results are carefully compared with those obtained from a reputable commercial FEM software, namely COMSOL. The optimized lamination parameter is then contrasted with the original unidirectional configuration to highlight the advantages of lamination

optimization. Through this comprehensive approach, the study ensures the soundness and validity of its findings.

By conducting this extensive research, the main objective is to make significant contributions to power optimization techniques in laminated composites integrated with piezoelectric patches. The study's outcomes will offer valuable insights into how lamination parameters affect energy harvesting performance, thereby supporting the creation of efficient and feasible energy harvesting systems. Ultimately, these advancements will align with the broader vision of achieving self-powered devices and promoting sustainable energy solutions across various engineering fields.

2. METHOD

2.1. Problem Definition

Piezoelectric materials are frequently used as patches or layers integrated onto the surfaces of flexible structures that have similarities to beams or plates. The diagram in Figure 2.1 provides a visual representation of a fully clamped composite plate, where a pair of piezo patches is attached in a bimorph configuration. The plate's dimensions are described by parameters a, b, and h_s, where a and b represent the length and width of the plate, respectively, and h_s is the overall thickness. The composite plate is composed of layers with consistent thickness for uniformity.

The piezo patches possess specific dimensions: l_p for length, w_p for width, and h_p for thickness. Both piezo-patches are symmetrically positioned relative to the plate's mid-plane and are affixed to the top and bottom surfaces of the laminated composite plate. This symmetrical attachment ensures a balanced and stable structure. The electrical connection of these piezo patches is designed in parallel and linked to a resistive load represented by R_l, enabling efficient power transfer and facilitating analysis.

To precisely locate the piezo patches, they occupy a designated rectangular region on the composite plate, defined by the coordinates of two corners, (x_1, y_1) and (x_2, y_2). These coordinates ensure accurate placement and alignment of the piezo patches for optimal performance.

For conducting frequency response analyses, a transverse harmonic point force is applied at specific coordinates (x_0, y_0), serving as the excitation source. This force stimulates the structure, allowing researchers to comprehensively study its frequency response characteristics. Such investigations yield valuable insights into the vibrational behavior of the plate, presenting opportunities energy harvesting.

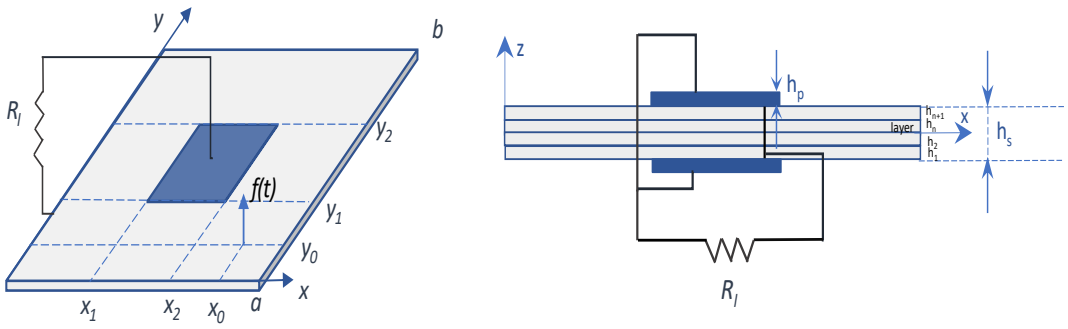

Figure 2.1: Schematic representation of a laminated composite plate with surface-bonded piezo patches: (a)Isometric view, (b) Cross-sectional view.

2.2. Constitutive Equations

Piezoelectric patches are commonly manufactured as thin plates, which allows for the adoption of a two-dimensional Kirchhoff plate model to describe their mechanical behavior. According to Kirchhoff plate theory, as explained by (Rao, 2007), this model makes the crucial assumption that the deflection of the middle surface is much smaller than the plate's thickness. Initially, the cross-sectional plane of the piezoelectric patch is perpendicular to the middle surface, and even during bending, this orientation remains unchanged. This simplification allows us to neglect the transverse shear strains (γ_{zx} and γ_{yz}), which represent deformations in directions perpendicular to the plate's surface.

Furthermore, the normal strain ε_{zz}, indicating deformation occurring in the thickness direction of the plate, can also be disregarded when analyzing transverse vibrations of the patch. This is justified by the thinness of the plate, which results in the normal stress σ_{zz} in the thickness direction being significantly smaller than the stresses occurring within the plane of the plate. Consequently, the plate can be treated as being in a plane stress state for transverse vibration analysis.

By employing the Kirchhoff plate model with these assumptions, researchers can effectively describe and analyze the mechanical response of the piezoelectric patch during various dynamic situations, leading to a better understanding of its behavior and enabling optimization for practical applications. Accordingly, the plane stress state:

$$\sigma_{zz} = \tau_{yz} = \tau_{zx} = 0 \tag{1}$$

In the framework of Kirchhoff plate theory, it is assumed that the structural layer material demonstrates orthotropic characteristics. This allows for the establishment of a relationship between stress and strain for a thin composite plate, which can be expressed as follows.

$$\begin{pmatrix} \sigma_{xx} \\ \sigma_{yy} \\ \tau_{xy} \end{pmatrix} = \begin{bmatrix} \frac{E_{11}}{1 - v_{21}v_{12}} & \frac{v_{21}E_{11}}{1 - v_{21}v_{12}} & 0 \\ \frac{v_{12}E_{22}}{1 - v_{21}v_{12}} & \frac{E_{22}}{1 - v_{21}v_{12}} & 0 \\ 0 & 0 & G_{12} \end{bmatrix} \begin{pmatrix} \varepsilon_{xx} \\ \varepsilon_{yy} \\ \gamma_{xy} \end{pmatrix} \tag{2}$$

In this context, Y_s denotes the Young's modulus, representing the measure of the structural layer's stiffness, while v_s refers to the Poisson's ratio, indicating the material's tendency to contract laterally when subjected to axial deformation.

After adopting a specific deformation theory, the subsequent step involves establishing a connection between the internal stresses and the applied loading, which is represented by stress resultants *{N}* and moment resultants *{M}*. Stress resultants signify the integrated stress across the thickness of the laminate, representing the applied force per unit width. Similarly, moment resultants denote the applied moment per unit width.

The principle of equilibrium is employed to equate the force and moment per unit width to the integral of the stress and the stress multiplied by the distance from the centerline. Figure 2.2 and Figure 2.3 illustrate the forces and moments according to the classical lamination theory. These representations and analyses are fundamental in understanding the mechanical response of laminated structures and are vital for designing optimized and efficient composite materials for various engineering applications.

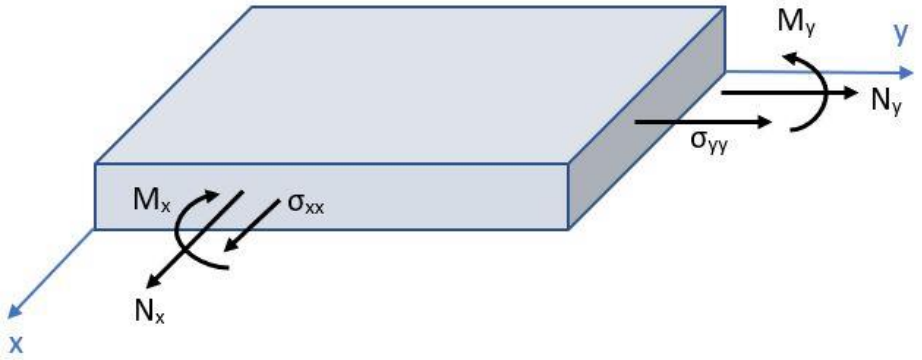

Figure 2.2. In plane normal forces and bending moment.

$$N_x = \int_{-h/2}^{h/2} \sigma_x \, dz \tag{3}$$

where *h* represents the plate's thickness, and *z* indicates the direction of thickness. When presented more concisely, the equation can be written as follows:

$$\begin{Bmatrix} N_x \\ N_y \\ N_{xy} \end{Bmatrix} = \int_{-h/2}^{h/2} \begin{Bmatrix} \sigma_x \\ \sigma_y \\ \tau_{xy} \end{Bmatrix} dz \tag{4}$$

The moment resultants can be compactly expressed as follows:

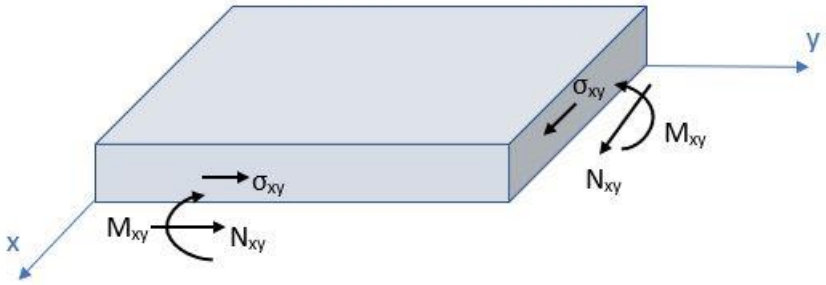

Figure 2.3. In- plane shear force and twisting moment.

$$\begin{Bmatrix} M_x \\ M_y \\ M_{xy} \end{Bmatrix} = \int_{-h/2}^{h/2} \begin{Bmatrix} \sigma_x \\ \sigma_y \\ \tau_{xy} \end{Bmatrix} z \, dz \tag{5}$$

In this context, the integration is conducted across the entire thickness of the laminate by summing up the integrals over each individual ply. Hence, the integrals are evaluated as follows, and Figure 2.4 illustrates the notation for the location of ply interfaces.

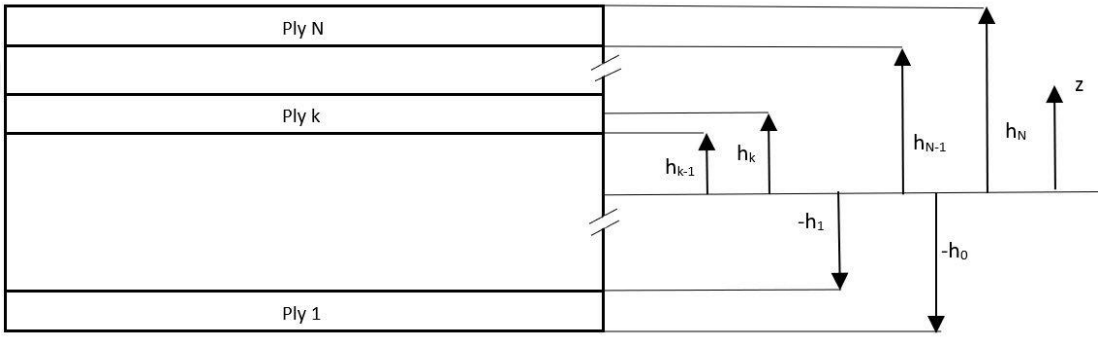

Figure 2.4. Notation for location of ply interfaces.

$$\begin{Bmatrix} N_x \\ N_y \\ N_{xy} \end{Bmatrix} = \sum_{k=1}^{N} \int_{h_{k-1}}^{h_k} \begin{Bmatrix} \sigma_x \\ \sigma_y \\ \tau_{xy} \end{Bmatrix} dz \tag{6}$$

$$\begin{Bmatrix} M_x \\ M_y \\ M_{xy} \end{Bmatrix} = \sum_{k=1}^{N} \int_{h_{k-1}}^{h_k} \begin{Bmatrix} \sigma_x \\ \sigma_y \\ \tau_{xy} \end{Bmatrix} zdz \tag{7}$$

By employing these integrals, the equations can be formulated in a conventional manner, establishing a relationship between stress resultants, moment resultants, centerline strains, and curvatures in the following expression:

$$\begin{Bmatrix} N \\ M \end{Bmatrix} = \begin{bmatrix} A & B \\ B & D \end{bmatrix} \begin{Bmatrix} \varepsilon^0 \\ K \end{Bmatrix} \tag{8}$$

The vector ε_0 represents the strains at the mid-plane, and K denotes the panel curvatures. A, B, and D are tensors representing the in-plane stiffness, in-plane/bending coupling, and bending stiffness, respectively. These tensors can be formulated based on the lamination parameters and material invariants.

Assuming a balanced and symmetric laminate, it becomes feasible to model the normalized in-plane stiffness tensor using just two lamination parameter variables. This can be expressed in the following manner (Tsai & Hahn, n.d.). The normalized lamination parameters, denoted as V_1 and V_3, can be defined as follows:

$$V_1 = \frac{1}{h}\sum_{k=1}^{N_l} t_k \cos(2\theta_k) \tag{9}$$

$$V_3 = \frac{1}{h}\sum_{k=1}^{N_l} t_k \cos(4\theta_k) \tag{10}$$

N_l represents the number of layers in the laminate, t_k's are the thicknesses of individual layers, and θ_k's are the angles of each layer. The material invariants, represented as U's, are computed using the following equation:

$$\begin{Bmatrix} U_1 \\ U_2 \\ U_3 \\ U_4 \\ U_5 \end{Bmatrix} = \begin{bmatrix} \frac{3}{8} & \frac{3}{8} & \frac{1}{4} & \frac{1}{2} \\ \frac{1}{2} & -\frac{1}{2} & 0 & 0 \\ \frac{1}{8} & \frac{1}{8} & -\frac{1}{4} & -\frac{1}{2} \\ \frac{1}{8} & \frac{1}{8} & \frac{3}{4} & -\frac{1}{2} \\ \frac{1}{8} & \frac{1}{8} & \frac{-1}{4} & \frac{1}{2} \end{bmatrix} \begin{Bmatrix} Q_{11} \\ Q_{22} \\ Q_{12} \\ Q_{66} \end{Bmatrix} \tag{11}$$

The reduced stiffness matrix entities, denoted as Q's, are determined by the following equation:

$$\begin{Bmatrix} Q_{11} \\ Q_{22} \\ Q_{12} \\ Q_{66} \end{Bmatrix} = \begin{Bmatrix} E_1/\gamma \\ E_2/\gamma \\ v_{12}E_2/\gamma \\ G_{12}/\gamma \end{Bmatrix} \tag{12}$$

$$\gamma = (1 - v_{12}v_{21}) \tag{13}$$

By utilizing the reciprocity relations for orthotropic layers, the Minor Poisson's ratio can be determined in the following manner:

$$v_{21} = \frac{v_{12}E_2}{E_1} \tag{14}$$

The connection between force and moment resultants and the strains in the laminate can be established by considering the material properties of each ply group. This relationship is commonly represented in the composite community using matrices labeled *A*, *B*, and *D*. For symmetric laminates, where the in-plane/bending coupling tensor is zero, the *B* matrix is also equal to zero (*B = 0*). Therefore, in symmetric laminates that are symmetric with respect to the mid-plane, the *B* matrix becomes negligible. By utilizing the normalized lamination parameters V_1 and V_3, as derived from equations [9] and [10], it becomes possible to express the normalized in-plane stiffness tensor.

$$\frac{A}{h} = \begin{bmatrix} U_1 & U_4 & 0 \\ U_4 & U_1 & 0 \\ 0 & 0 & U_5 \end{bmatrix} + \begin{bmatrix} U_2 & 0 & 0 \\ 0 & -U_2 & 0 \\ 0 & 0 & 0 \end{bmatrix} V_1 + \begin{bmatrix} U_3 & -U_3 & 0 \\ -U_3 & U_3 & 0 \\ 0 & 0 & -U_3 \end{bmatrix} V_3 \tag{15}$$

Furthermore, in the case of laminates composed of multiple uniformly distributed layers, the bending stiffness matrix approximates an orthotropic behavior, and it can be described using just two lamination parameter variables. This relationship is expressed as follows:

$$D = \frac{A\,h^2}{12} \tag{16}$$

The equations for the piezoelectric constant e_{31}, the dielectric permittivity at constant stress $\bar{\varepsilon}^{T}_{33}$, and the dielectric permittivity at constant strain $\bar{\varepsilon}^{S}_{33}$ are given as follows (*IEEE Standard on Piezoelectricity*, n.d.):

$$\bar{e}_{31} = \frac{d_{31}}{s_{11} + s_{12}} \tag{17}$$

$$\varepsilon^{S}_{33} = \bar{\varepsilon}^{T}_{33} - \frac{2d_{31}^2}{s_{11} + s_{12}} \tag{18}$$

The polarization direction of the piezoelectric patch is aligned with the z-axis. The parameter h_p represents the thickness of the piezoelectric patch, while $v_i(t)$ indicates the electrical potential difference (voltage output) generated by the ith piezoelectric patch in response to a specific vibration state. The electric field E_{33} is then utilized in subsequent steps for the following purposes:

$$E_{33} = -\frac{v_i(t)}{h_p} \tag{19}$$

As a consequence of the electric field's alignment with the *z*-axis, the electric displacement field *D* can be simplified to a scalar component, represented as D_3. For each piezo-patch, the stress and electric displacement components can be appropriately characterized using 2D constitutive equations, as extensively outlined in the research conducted by (Aridogan et al., 2014).

$$\begin{pmatrix} \sigma_{xx} \\ \sigma_{yy} \\ \tau_{xy} \\ {}_{D_3} \end{pmatrix} = \begin{bmatrix} \bar{c}_{11} & \bar{c}_{12} & 0 & -\bar{e}_{31} \\ \bar{c}_{12} & \bar{c}_{11} & 0 & -\bar{e}_{31} \\ 0 & 0 & \bar{c}_{66} & 0 \\ \bar{e}_{31} & \bar{e}_{31} & 0 & \bar{\varepsilon}^{s}_{33} \end{bmatrix} \begin{pmatrix} \varepsilon_{xx} \\ \varepsilon_{yy} \\ \gamma_{xy} \\ {}_{E_{33}} \end{pmatrix} \quad (20)$$

In this equation, the term c_{ij} represents the reduced modulus of elasticity associated with the piezoelectric patches. The equations of motion that govern the system are derived by applying Hamilton's principle, as exemplified in the research conducted by (Corrêa de Godoy & Areias Trindade, 2011).

$$\delta \oint_{t_1}^{t_2} \left(KE - PE + W_p\right) dt = 0 \quad (21)$$

Equation [21] represents a variant of Hamilton's principle, where δ denotes a variation in the system's configuration. In this equation, *KE* represents the system's kinetic energy, *PE* represents the system's potential energy, and W_p denotes the work done by non-conservative forces. The integral is taken over a specified time interval from t_1 to t_2. This equation states that the variation of the integral of the difference between kinetic energy (KE) and potential energy (PE), along with the work done by non-conservative forces (W_p), over the time interval is zero.

This principle reflects the concept that the actual motion of a system follows the path that minimizes the action, which is the integral of the Lagrangian function (KE-PE) over time. In other words, the system's motion follows the trajectory that yields the least action, combining both kinetic and potential energies, as well as accounting for non-conservative forces. This fundamental principle is a cornerstone in mechanics, providing a powerful framework for understanding and predicting the behavior of physical systems in various engineering and scientific applications.

The expression for the kinetic energy of the system can be derived as follows:

$$KE = \frac{1}{2}\iint_S m(x,y)\dot{w}^2\, dS \tag{22}$$

The parameter *S* represents the surface area of the system, encompassing both the upper surfaces of the piezo-patches and the thin composite plate. The variables *m(x,y)* and $\dot{w}$ represent the areal mass and velocity terms, respectively. The computation for determining the equivalent mass per unit area can be performed using the following expression:

$$m(x,y) = \rho_s h_s + \rho_p h_p P(x,y) \tag{23}$$

In this context, ρ_s and ρ_p represent the densities of the thin composite plate and the piezoelectric patch, respectively. The function *P(x,y)* acts as an indicator, identifying the specific locations on the surface of the composite plate where *k* piezoelectric patches have been attached. This function helps distinguish the regions where the piezoelectric patches are affixed, allowing for precise calculations of mass distribution and kinetic energy contributions in the system.

$$P(x,y) = \sum_{i=1}^{k}\left[H\left(x - x_{i,1}\right) - H\left(x - x_{i,2}\right)\right] \times \left[H\left(y - y_{i,1}\right) - H\left(y - y_{i,2}\right)\right] \tag{24}$$

Figure 2.5 depicts the geometrical parameters of the piezoelectric patch. The formula for calculating the area, defined by the four vertices x_1, x_2, y_1, and y_2 along the x and y-axes, along the x and y-axes, involves the utilization of the Heaviside unit step function denoted by *H*. This function enables the precise determination of the area by accounting for the specific vertices' coordinates, providing valuable information for further analysis and modeling of the piezoelectric patch's geometry and behavior.

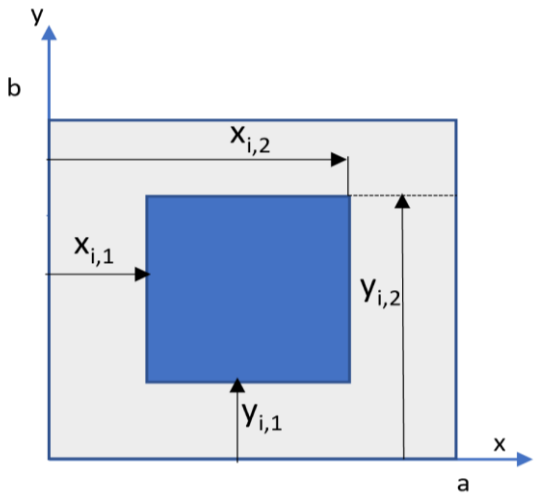

Figure 2.5. Representation of the geometric parameters of the piezoelectric patch.

The stored potential energy within the composite plate and piezoelectric patch is denoted by the symbol *PE*, and it can be expressed as follows:

$$PE = \frac{1}{2}\iiint_{V_s}\left\{(\sigma_{xx}\varepsilon_{xx})_s + (\sigma_{yy}\varepsilon_{yy})_s + (\tau_{xy}\gamma_{xy})_s\right\}dV_s + \frac{1}{2}\iiint_{V_p}\left\{(\sigma_{xx}\varepsilon_{xx})_p + (\sigma_{yy}\varepsilon_{yy})_p + (\tau_{xy}\gamma_{xy})_p\right\}dV_p \tag{25}$$

In this equation, the potential energy stored within the thin composite plate and the piezoelectric patch is determined by their respective volumes, denoted as V_s and V_p. The mathematical representation of the potential energy stored within the thin composite plate is as follows:

$$PE_S = \frac{1}{2}\iint_{S_s}\left\{D_{11}\left(\frac{\partial^2 w}{\partial x^2}\right)^2 + 2D_{12}\left(\frac{\partial^2 w}{\partial y^2}\right)\left(\frac{\partial^2 w}{\partial x^2}\right) + D_{22}\left(\frac{\partial^2 w}{\partial y^2}\right)^2 + 4D_{16}\left(\frac{\partial^2 w}{\partial x^2}\right)\left(\frac{\partial^2 w}{\partial x\partial y}\right) + 4D_{26}\left(\frac{\partial^2 w}{\partial y^2}\right)\left(\frac{\partial^2 w}{\partial x\partial y}\right) + 4D_{66}\left(\frac{\partial^2 w}{\partial x\partial y}\right)^2\right\}dS_s \tag{26}$$

The given equation involves two crucial elements: S_s, representing the surface area of a thin composite plate, and D_{ij}, which denotes the elements of the bending stiffness

matrix of a host plate comprising n layers. The derivation of these elements can be obtained through the following process:

$$D_{ij} = \frac{1}{3}\sum_{k=1}^{n}(Q_{ij})_k\,(z_k^3 - z_{k-1}^3), \qquad for\ i = j = 1,2,6 \tag{27}$$

The elements of the reduced stiffness matrix, labeled as Q_{ij}, can be determined by utilizing equations [12], [13], and [14]. The stored potential energy within the thin piezoelectric patches can be expressed by the following equation:

$$\begin{aligned} PE_P &= \frac{1}{2}\sum_{l=1}^{2}\iint_{S_p} P(x,y)\left\{D_{11}^{P}\left(\frac{\partial^2 w}{\partial x^2}\right)^2 + 2D_{12}^{p}\left(\frac{\partial^2 w}{\partial y^2}\right)\left(\frac{\partial^2 w}{\partial x^2}\right) + D_{11}^{p}\left(\frac{\partial^2 w}{\partial y^2}\right)^2\right. \\ &\left. + 4D_{66}^{p}\left(\frac{\partial^2 w}{\partial xy}\right)^2 - \bar{e}_{31}v(t)\left(\frac{h_s + h_p}{2}\right)\left(\frac{\partial^2 w}{\partial x^2} + \frac{\partial^2 w}{\partial y^2}\right)\right\} dS_p \end{aligned} \tag{28}$$

In this equation, S_p signifies the surface area of the piezoelectric patches, $v(t)$ represents the voltage applied to the patches, and D^p_{ij} corresponds to the bending stiffness matrix of the patches, which can be defined as follows:

$$D_{11}^{p} = \int_{\frac{h_s}{2}}^{\frac{h_s}{2}+h_p} \bar{c}_{11}\,z^2 dz = \int_{-\frac{h_s}{2}-h_p}^{-\frac{h_s}{2}} \bar{c}_{11}\,z^2 dz = \bar{c}_{11}\left(\frac{h_p^3}{3} + \frac{h_s^2 h_p}{4} + \frac{h_s h_p^2}{2}\right) \tag{29a}$$

$$D_{12}^{p} = \int_{\frac{h_s}{2}}^{\frac{h_s}{2}+h_p} \bar{c}_{12}\,z^2 dz = \int_{-\frac{h_s}{2}-h_p}^{-\frac{h_s}{2}} \bar{c}_{12}\,z^2 dz = \bar{c}_{12}\left(\frac{h_p^3}{3} + \frac{h_s^2 h_p}{4} + \frac{h_s h_p^2}{2}\right) \tag{29b}$$

$$D_{66}^{p} = \int_{\frac{h_s}{2}}^{\frac{h_s}{2}+h_p} \bar{c}_{66}\,z^2 dz = \int_{-\frac{h_s}{2}-h_p}^{-\frac{h_s}{2}} \bar{c}_{66}\,z^2 dz = \bar{c}_{66}\left(\frac{h_p^3}{3} + \frac{h_s^2 h_p}{4} + \frac{h_s h_p^2}{2}\right) \tag{29c}$$

The work done by the point force can be computed using the following equation:

$$W_p = \iint_S f(t)\delta(x - x0)\delta(y - y0)\, dS \tag{30}$$

In this equation, $f(t)$ denotes the amplitude of the force, while δ(x) and δ(y) represent the Dirac delta functions along the x and y axes, respectively. The displacement of the system is represented by *w*. By taking these variables into account, we can derive the equation of motion for the plate and piezoelectric patches in the following manner:

$$\begin{aligned} & m(x,y)\ddot{w} \\ & + \left[\begin{array}{c} \left\{D_{11} + P(x,y)2D_{11}^{p}\right\}\left(\frac{\partial^2 w}{\partial x^2}\right)^2 + \left\{\left(4D_{12}^{p}P(x,y) + 2D_{12}\right)\left(\frac{\partial^2 w}{\partial y^2}\right)\left(\frac{\partial^2 w}{\partial x^2}\right)\right\} \\ +(P(x,y)2D_{11}{}^{p} + D_{22})\left(\frac{\partial^2 w}{\partial y^2}\right)^2 + (4D_{16})\frac{\partial^2 w}{\partial x^2}\left(\frac{\partial^2 w}{\partial x \partial y}\right) \\ +(4D_{26})\left(\frac{\partial^2 w}{\partial y^2}\right)\left(\frac{\partial^2 w}{\partial x \partial y}\right) + \left(4D_{66} + 8D_{66}^{p}P(x,y)\right)\left(\frac{\partial^2 w}{\partial x \partial y}\right)^2 \end{array} \right] \\ & - \frac{2\ \bar{e}_{31}v(t)\left(h_s + h_p\right)}{2}P(x,y) * \left(\frac{\partial^2 w(x,y)}{\partial x^2} + \frac{\partial^2 w(x,y)}{\partial y^2}\right) \\ & = f(t)\delta(x - x0)\delta(y - y0) \end{aligned} \tag{31}$$

2.3. Miki's Lamination Diagram

Miki's Lamination Diagram is a valuable graphical tool extensively employed in the domain of composite materials to analyze and visualize the feasible design space for balanced and symmetric laminates. It was first introduced by (Miki, 1985). The diagram comprises two axes representing the normalized lamination parameters, usually denoted as V_1 and V_3. These parameters are calculated based on the angle and thickness of each layer within the laminate. By plotting different combinations of V_1 and V_3 values, engineers can effectively identify the allowable range of lamination configurations that meet specific design requirements. This diagram serves as a powerful aid in optimizing laminate designs for various engineering applications, ensuring the desired mechanical properties and structural integrity are achieved.

In Miki's Lamination Diagram, the feasible design region is visually represented by the interior and boundary areas. Points located within this region correspond to viable laminate designs that satisfy the balance and symmetry conditions. The boundary of the diagram is determined by a specific curve, which effectively separates the feasible area from the non-feasible area. This boundary curve serves as a critical reference, helping engineers distinguish between laminate configurations that meet the design criteria and those that do not. By analyzing the placement of points and the curve, designers can make informed decisions and select appropriate laminates that align with the desired mechanical properties and performance requirements.

$$V_3 = 2V_1^2 - 1 \tag{32}$$

Figure 2.6 displays Miki's Lamination Diagram, providing an insightful and visual representation. The diagram highlights specific points that correspond to laminates with orientations of [0°], $[\pm 45°]_s$,[90°], and $[0° \pm 45° 90°]_s$ (quasi–isotropic). These points represent different laminate configurations characterized by particular fiber angles. By examining the positions of these points on the diagram, engineers can quickly identify and assess the suitability of various laminates for specific structural applications. The diagram facilitates the efficient exploration of balanced and symmetric laminate designs, aiding in the selection of optimal configurations to meet the desired mechanical properties and performance criteria.

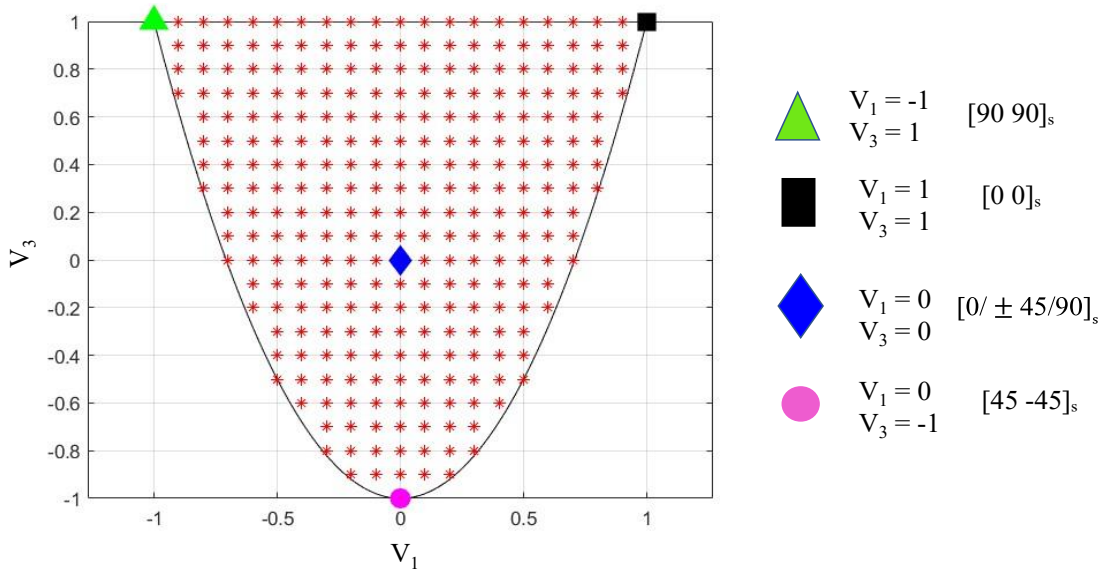

Figure 2.6: Miki's lamination diagram.

2.4. Modal Analysis

Modal analysis is a commonly used method to study the natural frequencies and mode shapes of a structure or system without considering external forces or damping effects. It allows for the exploration of the dynamic behavior of the structure and the identification of undamped natural frequencies and mode shapes. However, accurately analyzing the piezoelectric energy harvesting (PEH) patches presents challenges due to the presence of geometric inconsistencies at the edges of the piezoelectric patch. These inconsistencies can impact the accuracy of modal analysis results for such systems, making it necessary to develop specialized techniques to address these challenges.

To overcome this challenge, the Rayleigh-Ritz method has been utilized to perform modal vibration analysis of a laminated composite plate with integrated piezo-patches. The Rayleigh-Ritz method is a discretization technique commonly employed in engineering to approximate the natural frequencies and mode shapes of systems with distributed parameters. By applying fully clamped boundary conditions (CCCC), the method enables the determination of natural frequencies and their corresponding mode shapes for the system. This approach helps in accurately studying the dynamic behavior of the composite plate with piezo patches, taking into account the geometric

inconsistencies at the patch edges and providing valuable insights into its vibration characteristics.

To simplify the analysis, assumed modes are utilized to describe the displacement of the system, following the approach explained by (Yoon et al., 2016). This method enables a comprehensive exploration of the system's dynamic characteristics and offers valuable insights into its vibration behavior. By employing assumed modes, researchers can effectively model the complex interactions between the laminated composite plate and the integrated piezo patches, leading to a better understanding of the system's response to different vibration states.

$$w(x,y,t) = \sum_{i=1}^{R}\sum_{j=1}^{N} U_{ij}\, W_{ij}(x,y)\mu_{ij}(t) \tag{33}$$

In the given equation, $\mu_{ij}(t)$ signifies the generalized modal coordinates, which are linked to N vibration modes in the y coordinates and R vibration modes in the x coordinates. The analysis involves the use of assumed modes, denoted as $U_{ij}W_{ij}(x,y)$, where U_{ij} represents the corresponding coefficients, and $W_{ij}(x,y)$ represents the trial functions satisfying the boundary conditions. These assumed modes accurately capture the vibration patterns of the structure, allowing for an effective representation of the system's dynamic behavior. By employing these assumed modes, researchers can comprehensively examine and understand the vibrational characteristics of the laminated composite plate with integrated piezo patches, leading to precise predictions of its response to various vibration states.

To describe the shape of the vibration modes, orthogonal polynomials are utilized in both the x and y directions. These mathematical functions are mutually perpendicular and are employed to depict the characteristics of the vibration modes. The relationship between the vibration modes and the orthogonal polynomials can be expressed as demonstrated in the work by (Bhat, 1985). This mathematical representation allows for a thorough analysis of the structural vibration behavior, taking into account the interactions between different modes and their spatial distributions. By employing

orthogonal polynomials, researchers can effectively describe and understand the complex vibrational patterns exhibited by the laminated composite plate with integrated piezo patches, providing valuable insights into its dynamic response and aiding in optimizing its design and performance.

$$W_{ij(x,y)} = \phi_{i(x)} \cdot \varphi_{j(y)} \tag{34}$$

To obtain orthogonal polynomials within the interval $0 \leq x < a$, $0 \leq y < b$, the Gram-Schmidt procedure is employed. This method involves a systematic algorithm that takes an initial set of polynomials and transforms them into a new set of polynomials with orthogonality properties. Through the Gram-Schmidt procedure, the original set of polynomials is modified in such a way that each polynomial in the new set becomes orthogonal to all the other polynomials within the interval of interest. This procedure ensures that the resulting polynomials have distinct shapes and do not interfere with each other's contributions. By utilizing the Gram-Schmidt procedure, researchers can accurately represent the vibration modes of the laminated composite plate with integrated piezo-patches, providing a comprehensive understanding of its dynamic behavior and facilitating the analysis of the structural response to various excitation states.

$$\phi_2(x) = (x - B_2)\phi_1(x), \qquad \phi_r(x) = (x - B_r)\phi_{r-1}(x) - C_r\phi_{r-2}(x) \tag{35a}$$

$$B_r = \frac{\int_0^a xk(x)\phi_{r-1}^2(x)dx}{\int_0^a k(x)\phi_{r-1}^2(x)dx} \tag{35b}$$

$$C_r = \frac{\int_0^a xk(x)\phi_{r-1}(x)\phi_{r-2}(x)dx}{\int_0^a k(x)\phi_{r-2}^2(x)dx} \tag{36}$$

In this equation, a polynomial function is multiplied by a weighting function denoted as *k(x)*. For this specific case, the decision was made to utilize the unit weighting function, and the coefficients of the polynomial functions were then determined to satisfy the orthonormal condition. By employing the unit weighting function, the focus

is on finding the appropriate coefficients of the polynomial functions, ensuring that the resulting set of orthogonal polynomials is both normalized and mutually orthogonal within the specified interval. This approach allows for an accurate representation of the vibration modes of the laminated composite plate with integrated piezo-patches, facilitating a comprehensive analysis of its dynamic behavior.

$$\int_0^a \phi_r(x)\phi_f(x)dx = \begin{cases} 0 & if \quad r \neq f \\ 1 & if \quad r = f \end{cases} \tag{37}$$

The boundary condition of a rectangular beam with fixed-fixed ends, which is characterized by the first term of the orthogonal polynomials denoted as $\phi_1(x)$, can be obtained using specific techniques as outlined in the work by (Yoon et al., 2016). This mathematical expression represents the mathematical representation of the fixed-fixed boundary condition for the beam with a length of a.

$$\phi_1(x) = a^2x^2 - 2ax^3 + x^4, \ \ (0 \leq x \leq a) \tag{38a}$$

$$\varphi_1(x) = b^2y^2 - 2by^3 + y^4, \ \ (0 \leq y \leq b) \tag{38b}$$

Rayleigh's quotient, denoted as U_{ij}, can be defined as the ratio between the maximum potential energy and the corresponding reference kinetic energy (Meirovitch, 2001). This expression provides a quantitative measure of the relationship between potential energy and kinetic energy within a system. By evaluating this quotient, researchers can gain insights into the energy distribution and dynamic behavior of the system, which is crucial for understanding its vibration characteristics and stability.

$$R\left[U_{ij}W_{ij}(x,y)\right] = \frac{PE_{max}}{KE_{ref}} \tag{39}$$

To determine the conditions for achieving a stationary value of Rayleigh's quotient, it is essential to take its derivative with respect to the coefficients U_{rn}. This differentiation process will provide the crucial conditions that must be fulfilled for

obtaining a stationary value. By equating the derivative to zero, researchers can identify the critical points where the potential energy reaches its maximum or minimum, allowing for the exploration of the system's stable equilibrium configurations or natural frequencies in the context of vibration analysis.

$$\frac{\partial R}{\partial U_{ij}} = \left(\frac{\partial PE_{max}}{\partial U_{ij}} - \omega_{ij}^2 \frac{\partial KE_{ref}}{\partial U_{ij}} \right) = 0 \tag{40}$$

The maximum potential energy (PE_{max}) and the reference kinetic energy (KE_{ref}) can be obtained using the following equations, which provide the expressions for calculating these quantities.

$$PE_{max} = \frac{1}{2} \sum_{i=1}^{N} \sum_{j=1}^{N} \sum_{k=1}^{N} \sum_{l=1}^{N} K_{ij,kl} U_{ij} U_{kl} \tag{41}$$

$$KE_{ref} = \frac{1}{2} \sum_{i=1}^{N} \sum_{j=1}^{N} \sum_{k=1}^{N} \sum_{l=1}^{N} M_{ij,kl} U_{ij} U_{kl} \tag{42}$$

To compute the stiffness term, $K_{ij,kl}$, the following procedure can be utilized:

43

$$\begin{aligned} K_{ij,kl} = \iint_S [& \left\{ D_{11} + 2D_{11}^p P(x,y) \right\} \left[\frac{\partial^2 W_{ij}}{\partial x^2} \frac{\partial^2 W_{kl}}{\partial x^2} \right] \\ & + \left\{ D_{12} + 2D_{12}^p P(x,y) \right\} \left[\frac{\partial^2 W_{ij}}{\partial x^2} \frac{\partial^2 W_{kl}}{\partial y^2} + \frac{\partial^2 W_{ij}}{\partial y^2} \frac{\partial^2 W_{kl}}{\partial x^2} \right] \\ & + \{2D_{16}\} \left[\frac{\partial^2 W_{ij}}{\partial x^2} \frac{\partial^2 W_{kl}}{\partial xy} + \frac{\partial^2 W_{ij}}{\partial xy} \frac{\partial^2 W_{kl}}{\partial x^2} \right] \\ & + \left\{ D_{22} + 2D_{11}^p P(x,y) \right\} \left[\frac{\partial^2 W_{ij}}{\partial y^2} \frac{\partial^2 W_{kl}}{\partial y^2} \right] \\ & + \{2D_{26}\} \left[\frac{\partial^2 W_{ij}}{\partial y^2} \frac{\partial^2 W_{kl}}{\partial xy} + \frac{\partial^2 W_{ij}}{\partial xy} \frac{\partial^2 W_{kl}}{\partial y^2} \right] \\ & + \left\{ 4D_{66} + 8D_{66}^p P(x,y) \right\} \left[\frac{\partial^2 W_{ij}}{\partial xy} \frac{\partial^2 W_{kl}}{\partial xy} \right]] dS \end{aligned}$$

To obtain the mass term, $M_{ij,kl}$, the following approach can be employed:

$$M_{ij,kl} = \iint_S W_{ij}(x,y)m(x,y)W_{kl}(x,y)dS \tag{44}$$

Once the mass and stiffness parameters have been computed, the eigenvalue problem for analyzing the natural vibration of piezoelectric patches can be formulated as follows:

$$\left[K_{ij,kl} - \omega_{ij}^2 M_{ij,kl}\right]\left[U_{ij}\right] = \{0\} \tag{45}$$

In this formulation, the eigenvectors of the equation, represented by U_{ij}'s, correspond to the coefficients of the assumed mode shapes. The corresponding eigenvalues of the equation are the squares of the natural frequencies, denoted as ω_{ij}'s. These eigenvalues provide valuable information about the system's vibrational behavior, indicating the frequencies at which the laminated composite plate with integrated piezo patches will naturally vibrate without external excitations.

2.5. Electrical Circuit Equations

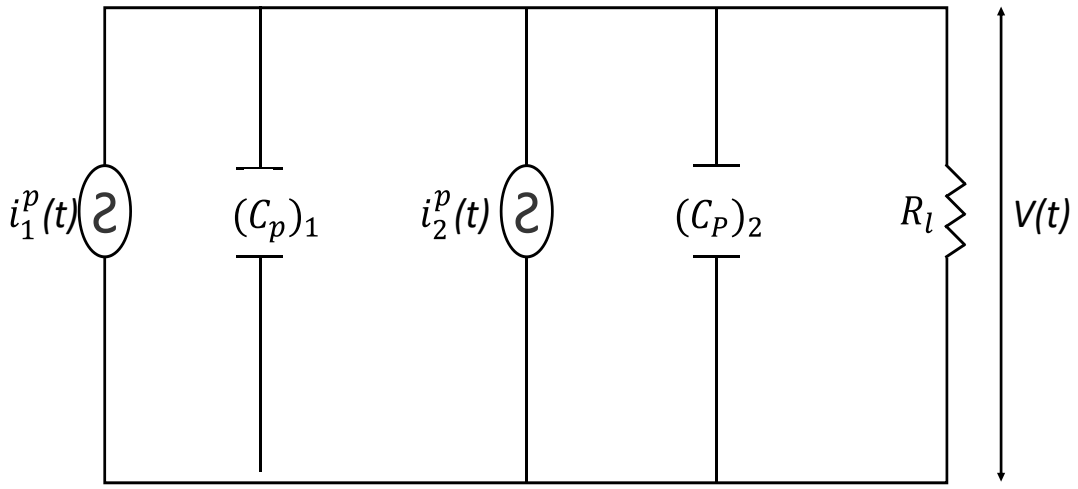

Figure 2.7: The representation of the electromechanical system in terms of an equivalent circuit.

Figure 2.7 depicts the representation of two piezo patches connected to a resistive load in the form of an equivalent circuit. It is worth noting that when nonlinear circuits are employed alongside the piezo-patches, an alternative approach called the equivalent impedance method can be utilized, as proposed by (Motlagh et al., 2020). By applying Kirchhoff's current law, the circuit equation can be formulated as follows:

$$\frac{dv(t)}{dt}\sum_{l=1}^{N}(C_P)_l + \frac{v(t)}{R_l} = \sum_{l=1}^{N} i_l^{\mathrm{p}}(t) \ \ (N = 1,2,\ldots number\ of\ patches) \tag{46}$$

In this equation, the term $i_l^{\mathrm{p}}(t)$ represents the current source dependent on the velocity, $(C_p)_l$ denotes the equivalent capacitance of the lth piezo-patch, and θ_l corresponds to the electromechanical coupling term for the lth piezo-patch. The value of θ_l can be determined through the following procedure.

$$i_l^{\mathrm{p}}(t) = -\theta_l \frac{\partial}{\partial t}\iint_{S_p}\left(\frac{d^2w}{dx^2} + \frac{d^2w}{dy^2}\right)dS_p \tag{47}$$

$$\left(C_p\right)_l = (\bar{\varepsilon}_{33}^{S})\frac{(l_p)(w_p)}{h_p} \tag{48}$$

$$\theta_l = \bar{e}_{31}\left(\frac{h_s + h_p}{2}\right) \tag{49}$$

2.6. Harmonic Point Force Excitation and Its Steady-state Responses

By utilizing a transformation procedure that incorporates modal coordinates, the system's equations as represented in equation (31) in physical coordinates can be effectively converted into modal coordinates. It has been clarified by (Yoon et al., 2016) that the assumed mode shape coefficients U_{ij} exhibit orthogonality with respect to the mass and stiffness matrices. This inherent orthogonality property leads to a decoupling effect, resulting in uncoupled equations of motion when the system's equations are transformed from physical coordinates to modal coordinates. This

decoupling simplifies the analysis and allows for the independent examination of each mode, enabling a clearer understanding of the system's dynamic response to different vibration modes.

$$M'_{ij,kl} = U_{ij}^{T} M_{ij,kl} U_{kl} = \begin{cases} 1 & if \;\; ij = kl \\ 0 & if \;\; ij \neq kl \end{cases} \tag{50}$$

$$K'_{ij,kl} = U_{ij}^{T} K_{ij,kl} U_{kl} \;\; = \begin{cases} \omega_{ij}^{2} & if \quad ij = kl \\ 0 & if \quad ij \neq kl \end{cases} \tag{51}$$

The modal mass and stiffness matrices, represented as $M'_{ij,kl}$ and $K'_{ij,kl}$, respectively, are essential components in the modal coordinate representation. To calculate the applied point force in modal coordinates, a specific procedure must be carried out, involving a series of calculations or computations. This process is necessary to transform the applied force from physical coordinates to modal coordinates, allowing for a more convenient and efficient analysis of the system's dynamic response in terms of its natural modes of vibration.

$$\begin{aligned} f_{rs} = \quad & \iint_{S} f(t)\delta(x - x0)\delta(y - y0) U_{rs} W_{rs}(x, y) dS \\ & = f(t) U_{rs} W_{rs}(x0, y0) \\ & r = 1,2,3, \dots, N \quad s = 1,2,3, \dots, N \end{aligned} \tag{52}$$

The current output in modal coordinates can be determined by following the subsequent procedure or method.

$$i_{l}^{\mathrm{p}}(t) \;\; = -\sum_{r=1}^{N} \sum_{s=1}^{N} \frac{d\mu_{rs}(t)}{dt} \left(\tilde{\theta}_{rs}\right)_{l} \tag{53}$$

The following expression can be used to represent the electromechanical coupling term $\left(\tilde{\theta}_{rs}\right)_{l}$ of the *l*th piezo patch in modal coordinates:

$$\left(\tilde{\theta}_{rs}\right)_l = \theta_l \iint_{S_p} U_{rs} P(x,y) \left(\frac{d^2 W_{rs}}{dx^2} + \frac{d^2 W_{rs}}{dy^2}\right) dS_p \tag{54}$$

The electromechanically coupled equations of the system can be represented in modal coordinates as shown in the following manner, as demonstrated by (Gohari et al., 2016):

$$\frac{\partial^2 \mu_{rs}(t)}{\partial t^2} + 2\omega_{rs}\zeta_{rs}\frac{\partial \mu_{rs}(t)}{\partial t} + \omega_{rs}^2 \mu_{rs}(t) - \sum_{l=1}^{2}\left(\tilde{\theta}_{rs}\right)_l v(t) = f_{rs}(t) \tag{55}$$

$$\frac{dv(t)}{dt}\sum_{l=1}^{2}\left(C_p\right)_l + \frac{v(t)}{R_l} + \sum_{l=1}^{2}\sum_{r=1}^{N}\sum_{s=1}^{N}\frac{d\mu_{rs}(t)}{dt}\left(\tilde{\theta}_{rs}\right)_l = 0 \tag{56}$$

For a linear system, when a harmonic force input is applied in the form of $f(t) = F_0 e^{j\omega t}$, the resulting steady-state voltage output and mechanical modal response can be expressed as follows, taking into account ω_{rs} as the natural frequency and ζ_{rs} as the modal damping ratio:

$$v(t) = V e^{j\omega t} \tag{57}$$

$$\mu_{rs}(t) = H_{rs} e^{j\omega t} \tag{58}$$

Within this context, *V* represents the complex magnitude of the voltage output, and H_{rs} denotes the complex amplitude of the modal response. By substituting the values of $\mu_{rs}(t)$, $v(t)$, and f_{rs} into the equations, one can compute the complex modal amplitude H_{rs}

$$H_{rs} = \frac{F_0 U_{rs} W_{rs}(x0, y0) + V \sum_{l=1}^{2} \left(\tilde{\theta}_{rs}\right)_l}{\omega_{rs}^2 - \omega^2 + 2j\zeta_{rs}\omega_{rs}\omega} \tag{59}$$

Using a similar substitution approach, one can determine the complex voltage amplitude *V*.

$$V = \frac{-\sum_{l=1}^{2}\sum_{r=1}^{N}\sum_{s=1}^{N} \frac{j\omega\left(\tilde{\theta}_{rs}\right)_l F_0 U_{rs} W_{rs}(x0, y0)}{\omega_{rs}^2 - \omega^2 + 2j\zeta_{rs}\omega_{rs}\omega}}{j\omega \sum_{l=1}^{2}\left(C_p\right)_l + \frac{1}{R_l} + \sum_{l=1}^{2}\sum_{r=1}^{N}\sum_{s=1}^{N} \frac{j\omega\left(\tilde{\theta}_{rs}\right)_l \sum_{l=1}^{2}\left(\tilde{\theta}_{rs}\right)_l}{\omega_{rs}^2 - \omega^2 + 2j\zeta_{rs}\omega_{rs}\omega}} \tag{60}$$

By employing a substitution technique similar to the equation, the modal displacement of the system in modal coordinates can be determined.

$$w(x, y, t) = \sum_{r=1}^{N}\sum_{s=1}^{N}\left(\frac{U_{rs} W_{rs}(x, y)\left[F_0 U_{rs} W_{rs}(x0, y0) + V \sum_{l=1}^{2}\left(\tilde{\theta}_{rs}\right)_l\right] e^{j\omega t}}{\omega_{rs}^2 - \omega^2 + 2j\zeta_{rs}\omega_{rs}\omega}\right) \tag{61}$$

By applying a harmonic force input, it becomes feasible to calculate the frequency response function of the voltage, which illustrates the relationship between the input force and the resulting voltage output.

$$\frac{v(t)}{F_0 e^{j\omega t}} = \frac{-\sum_{l=1}^{2}\sum_{r=1}^{N}\sum_{s=1}^{N} \frac{j\omega\left(\tilde{\theta}_{rs}\right)_l U_{rs} W_{rs}(x0, y0)}{\omega_{rs}^2 - \omega^2 + 2j\zeta_{rs}\omega_{rs}\omega}}{j\omega \sum_{l=1}^{2}\left(C_p\right)_l + \frac{1}{R_l} + \sum_{l=1}^{2}\sum_{r=1}^{N}\sum_{s=1}^{N} \frac{j\omega\left(\tilde{\theta}_{rs}\right)_l \sum_{l=1}^{2}\left(\tilde{\theta}_{rs}\right)_l}{\omega_{rs}^2 - \omega^2 + 2j\zeta_{rs}\omega_{rs}\omega}} \tag{62}$$

In similar way, by subjecting the system to a harmonic force input, connection between the input force and modal displacement of the system can be written by following equation.

$$\frac{w(x,y,t)}{F_0 e^{j\omega t}} = \sum_{r=1}^{N}\sum_{s=1}^{N}\left(\frac{U_{rs}W_{rs}(x,y)\left[U_{rs}W_{rs}(x0,y0) + \alpha(\omega)\sum_{l=1}^{2}\left(\tilde{\theta}_{rs}\right)_l\right]}{\omega_{rs}^2 - \omega^2 + 2j\zeta_{rs}\omega_{rs}\omega}\right) \quad (63)$$

2.7. Technique For Separating Integrals

In the previous section, we discussed the modal analysis solution of a composite plate coupled with piezo patches using the Rayleigh-Ritz method. However, this method involved a surface integral operation, leading to substantial computational time, particularly when dealing with large mode numbers. In this section, we introduce an alternative technique that involves splitting the integrals, effectively dividing the surface integral into two separate integrals. By employing this method, a notable reduction in computational time can be attained, especially in scenarios involving higher mode numbers.

The variables ε and η denote dimensionless quantities along the *x* and *y* coordinates, respectively, as represented by the following expressions:

$$\varepsilon = {}^{x}/_{a} \qquad \eta = {}^{y}/_{b} \quad (64)$$

The understanding of the system's displacement in physical coordinates can be clarified by examining the normalized variables and their importance in characterizing the displacement field, as explained by (Bhat, 1985).

$$w(\varepsilon,\eta,t) = \sum_{m=1}^{N}\sum_{n=1}^{N} U_{mn}X_m(\varepsilon)Y_n(\eta)\mu_{mn}(t) \quad (65)$$

Using normalized variables, the *x* and *y* coordinates can be represented as orthogonal polynomials $X_m(\varepsilon), Y_n(\eta)$. These polynomials are defined by the coefficient U_{mn} and

generalized modal coordinates $\mu_{mn}(t)$. Additionally, the indicator function $P(\varepsilon,\eta)$ can be separated into two distinct components.

$$P(\varepsilon,\eta) = P\mathrm{x}(\varepsilon).P\mathrm{y}(\eta) \tag{66a}$$

$$P\mathrm{x}(\varepsilon) = [H(\varepsilon - x_1/a) - H(\varepsilon - x_2/a)] \tag{66b}$$

$$P\mathrm{y}(\eta) = \left[H\left(\eta - \frac{y_1}{b}\right) - H\left(\eta - \frac{y_2}{b}\right)\right] \tag{66c}$$

The existence of $P\mathrm{x}(\varepsilon)$ and $P\mathrm{y}(\eta)$ signifies separate Heaviside-step functions operating in the *x* and *y* directions, which depend on the normalized variables ε and η. By substituting equation (65) into equations (40), (41), and (42), an eigenvalue equation similar to equation (45) can be derived.

$$\sum_{m=1}^{N}\sum_{n=1}^{N}[C_{mnij} - \lambda M_{mnij}]U_{mn} = 0 \tag{67}$$
$$\lambda = \rho_s h_s {\omega_{mn}}^2 a^4/D_{11}$$

The stiffness term C_{mnij} represents the interaction between the host structure and the piezo-patches and can be expressed as follows:

$$C_{mnij} = Cs_{mnij} + 2Cp_{mnij} \tag{68}$$

The expressions denoting the stiffness term of the host structure Cs_{mnij} and the piezo patches Cp_{mnij} can be formulated as follows:

$$\begin{aligned} Cs_{mnij} = {} & E_{mi}^{(2,2)}F_{nj}^{(0,0)} + \alpha^4 E_{mi}^{(0,0)}F_{nj}^{(2,2)}\left(\frac{D_{22}}{D_{11}}\right) \\ & +\alpha^2\left[E_{mi}^{(0,2)}F_{nj}^{(2,0)} + E_{mi}^{(2,0)}F_{nj}^{(0,2)}\right]\left(\frac{D_{12}}{D_{11}}\right) \\ & +2\alpha\left[E_{mi}^{(2,1)}F_{nj}^{(0,1)} + E_{mi}^{(1,2)}F_{nj}^{(1,0)}\right]\left(\frac{D_{16}}{D_{11}}\right) \end{aligned} \tag{69}$$

$$+2\alpha^3\left[E_{mi}^{(0,1)}F_{nj}^{(2,1)}+E_{mi}^{(1,0)}F_{nj}^{(1,2)}\right]\left(\frac{D_{26}}{D_{11}}\right)+4\alpha^2E_{mi}^{(1,1)}F_{nj}^{(1,1)}\left(\frac{D_{66}}{D_{11}}\right)$$

$$Cp_{mnij}=Ep_{mi}^{(2,2)}Fp_{nj}^{(0,0)}\left(\frac{D_{11}^{p}}{D_{11}}\right)+\alpha^4Ep_{mi}^{(0,0)}Fp_{nj}^{(2,2)}\left(\frac{D_{22}^{p}}{D_{11}}\right) \tag{70}$$
$$+\alpha^2\left[E_{mi}^{(0,2)}F_{nj}^{(2,0)}+E_{mi}^{(2,0)}F_{nj}^{(0,2)}\right]\left(\frac{D_{12}}{D_{11}}\right)+4\alpha^2Ep_{mi}^{(1,1)}Fp_{nj}^{(1,1)}\left(\frac{D_{66}^{p}}{D_{11}}\right)$$

The aspect ratio (α=a/b) describes the proportions of the host structure, while the mass term M_{mnij} considers the combined mass contributions from both the host structure and the piezo patches.

$$M_{mnij}=Ms_{mnij}+2Mp_{mnij}\ \rho_ph_p/\rho_sh_s \tag{71}$$

In this equation, the mass term of the host structure $Ms_{mnij}$and the piezo patch Mp_{mnij} can be expressed using the following equations:

$$Ms_{mnij}=E_{mi}^{(0,0)}F_{nj}^{(0,0)} \tag{72}$$

$$Mp_{mnij}=Ep_{mi}^{(0,0)}Fp_{nj}^{(0,0)} \tag{73}$$

The host structure components $E_{mi}^{(r,s)}$, $F_{nj}^{(r,s)}$ and the piezo patch components $Ep_{mi}^{(r,s)}$,$Fp_{nj}^{(r,s)}$ are given by the following expressions:

$$E_{mi}^{(r,s)}=\int_0^1\frac{\partial^rX_m(\varepsilon)}{\partial\varepsilon^r}\frac{\partial^sX_i(\varepsilon)}{\partial\varepsilon^s}d\varepsilon \tag{74}$$

$$F_{nj}^{(r,s)}=\int_0^1\frac{\partial^rY_n(\varepsilon)}{\partial\eta^r}\frac{\partial^sY_j(\eta)}{\partial\eta^s}d\eta \tag{75}$$

$$Ep_{mi}^{(r,s)}=\int_0^1Px(\varepsilon)\frac{\partial^rX_m(\varepsilon)}{\partial\varepsilon^r}\frac{\partial^sX_i(\varepsilon)}{\partial\varepsilon^s}d\varepsilon \tag{76}$$

$$Fp_{nj}^{(r,s)} = \int_0^1 Py(\eta) \frac{\partial^r Y_n(\varepsilon)}{\partial \eta^r} \frac{\partial^s Y_j(\eta)}{\partial \eta^s} \, d\eta \tag{77}$$

$$where\ m, i = 1,2,3, \dots, N \quad n, j = 1,2,3, \dots, N \qquad r, s = 0,1,2$$

The equation (67) allows us to find the eigenvalues (λ) and eigenvectors (U_{mn}), which are crucial for understanding the behavior of the system. The natural frequencies ω_{mn} can be determined by solving equation (67). It is important to note that, for harmonic response, the modal mass and stiffness matrices can be obtained by substituting equations (68) and (71) into equation (50) and equation (51), respectively. By replacing $U_{mn}X_m(\varepsilon)Y_n(\eta)$ with $U_{rs}W_{rs}(x, y)$ in equations (52) and (53) and using the separation of integrals, we can calculate the applied force and electromechanical coupling term in modal coordinates. Consequently, the governing equations of motion in modal coordinates can be derived. The same approach discussed in the previous section can be applied to compute the displacement, voltage outputs, and their frequency response functions in modal coordinates.

2.8. Finite Element Modelling

The study conducted modal and harmonic analyses for different panel geometries and lamination parameters using finite element analyses (FEA). To validate the accuracy of the analytical model's results, comparisons were made with simulations performed using COMSOL, a commercial FEA software. Special interface constraint equations were formulated to ensure proper bonding between the host structure and the piezoelectric patches. The connection between the piezo-patches and the external resistive load was represented using a piezoelectric circuit element. Modal analysis was carried out to determine the mode shapes and natural frequencies. Utilizing the mode superposition method and considering the first 10 vibration modes, the voltage and displacement frequency response functions (FRFs) were computed.

2.9. Optimization of Power Output

The calculation of the multi-mode power output can be obtained using the following equation. In this equation, *V* signifies the voltage output generated by the piezo-

patches, and R_l denotes the resistance of the load connected to the circuit. The multi-mode power output is a crucial parameter that reflects the electrical energy generated by the piezoelectric system under various vibration modes and frequencies. By considering the voltage output and the load resistance, engineers can assess the efficiency and performance of the energy harvesting system across different operating conditions.

$$Power\ Output\ = \frac{V^2}{R_l} \tag{78}$$

The given equation enables the determination of the load resistance, R_l, by considering the capacitance C_{pc} and the system's first natural frequency (ω_1). This equation provides a means to calculate the appropriate load resistance value that optimizes the power output of the piezoelectric system. The capacitance C_{pc} and the first natural frequency are crucial factors in determining the system's electrical behavior and efficiency.

$$R_l = \frac{1}{Cpc * \omega_1.} \tag{79}$$

3. RESULT AND DISCUSSION

3.1. Analytical Model Validation Using Finite Element Analysis

The results obtained from an analytical model of composite plates with symmetrical piezo patches were analyzed and validated to assess its accuracy. The validation studies involved comparing the model's predictions for natural frequencies, mode shapes, displacement, and voltage frequency response functions (FRFs) with results obtained from finite element analysis (FEA). Detailed material properties for both the composite plate and piezo patches are listed in Table 3.1, providing comprehensive information for the analytical model's evaluation.

Table 3.1: Material properties of composite plate and piezo-patches.

Properties	Composite Plate	Piezoelectric Material
Width(mm)	500	150
Length(mm)	500	150
Thickness(mm)	2,5	0,2
Mass Density(kg/m^3)	1500	7750
Poisson's Ratio	0,25	0,35
Piezoelectic Constant $\bar{e}_{31}$ [C/m^2]	-	-16,041
Permittivity Constant $\bar{\varepsilon}^s_{33}$ [nF/m]	-	9,56
Young Modulus (E_{11}) [GPa]	150	-
Transverse Elastic Modulus (E_{22}) [GPa]	10	-
Shear Elastic Modulus G_{12} [GPa]	6	-
Piezoelectric strain coefficient (d_{31})	-	-171 pm V^{-1}
Dielectric permittivity at constant strain (ε^s_{33})	-	9,5657 nF m^{-1}
Dielectric permittivity at constant stress (ε^T_{33})	-	1,5052 nF m^{-1}
Absolute permittivity (ε_0)	-	8,854 pF m^{-1}
Compliances of the piezoelectric patch	-	S_{11}:16,4 pm^2 N^{-1} S_{12}:5,74 pm^2 N^{-1} S_{66} :44,3 pm^2 N^{-1}

3.2. Natural Frequencies of System

The modal analysis of composite plates with surface-bonded piezo-patches is conducted using two distinct approaches: the Rayleigh-Ritz method and finite element simulations. The utilization of these complementary techniques allows for a comprehensive examination of the structural behavior. The outcomes of the modal analysis are meticulously documented in Table 3.2, presenting a detailed account of the initial ten resonance frequencies exhibited by the system. A wide-ranging exploration is undertaken, exploring diverse combinations of four ply angles within both 4-layer laminated plates, all of which are intricately integrated with surface-bonded piezo patches. This exhaustive analysis aims to capture the rich diversity of potential configurations and gain insights into the influence of ply orientations on the vibrational characteristics of the composite plate, thereby enabling the identification of optimal designs to meet specific engineering requirements.

Table 3.2: First ten natural frequency for the different four lamination parameters

V_1=1, V_3=1 $[0/0]_s$			V_1=0, V_3= -1 $[45/-45]_s$			V_1= -1, V_3=1 $[90/90]_s$			V_1=0, V_3=0 $[0/\pm45/90]_s$		
R-R	FEM	Diff. (%)	R-R	FEM	Diff. (%)	R-R	FEM	Diff. (%)	R-R	FEM	Diff. (%)
98,79	98,63	0,17	91,08	91,11	0,04	98,79	98,63	0,17	97,65	97,70	0,05
134,2	133,5	0,57	175,7	175,7	0,02	134,2	133,5	0,57	170,10	169,96	0,08
207,9	208,8	0,38	213,5	213,7	0,12	207,9	208,8	0,38	249,60	249,89	0,12
277,5	277,6	0,03	283,1	283,9	0,32	277,5	277,6	0,03	286,47	288,01	0,54
301,9	297,1	1,65	348,5	350,1	0,46	301,9	297,1	1,65	323,22	323,91	0,21
309,6	310,0	0,11	373,0	374,3	0,35	309,6	310,0	0,11	414,54	415,38	0,20
352,2	353,1	0,25	399,1	399,9	0,22	352,2	353,1	0,25	450,94	451,52	0,13
422,7	422,1	0,14	485,2	487,0	0,37	422,7	422,1	0,14	475,14	475,91	0,16
426,4	422,9	0,83	536,4	537,7	0,25	426,4	422,9	0,83	544,67	545,38	0,13
528,8	530,7	0,34	551,4	553,4	0,37	528,8	530,7	0,35	557,99	559,46	0,26

The abbreviation "R-R" refers to the Rayleigh-Ritz method, which is a powerful analytical technique utilized for modal analysis. The subsequent columns in the presented table showcase the outcomes obtained from the analytical solution based on this method. On the other hand, "FEA" stands for the finite element method, and the following columns illustrate the results obtained using COMSOL, a widely used commercially available finite element analysis software. Throughout the extensive analysis performed, it is important to highlight that all scenarios considered involve the strategic placement of piezo patches at the center of the composite plate. This positioning allows for the investigation of the most critical vibrational characteristics of the structure, ensuring that the effects of the piezo patches on the plate's dynamic behavior are thoroughly assessed.

In conducting a meticulous comparison between the analytical model and the COMSOL model, it is observed that the results exhibit a remarkable level of agreement, with the discrepancy between the two approaches amounting to no more than 1%. This close correspondence validates the accuracy and reliability of the analytical model in capturing the vibrational behavior of the composite plate coupled with surface-bonded piezo-patches.

Table 3.3 showcases the first six mode shapes of the composite plate system, with a focus on investigating various combinations of four ply angles within a laminated structure comprising four layers and surface-bonded piezo-patches. This comprehensive analysis aims to explore the influence of different ply orientations on the mode shapes and their associated vibrational patterns. In Table 3.3, the first column serves as a mode number reference, facilitating the identification and correlation of specific mode shapes. The subsequent columns display the mode shapes corresponding to different lamination arrays. These arrays are represented by ply angle configurations, namely, 0/0/0/0, 45/45/45/45, 90/90/90/90, and -45/45/45/-45. Each lamination array represents a unique arrangement of fiber orientations in the composite plate. By analyzing the mode shapes for each lamination array, valuable insights are gained into the distinct vibration patterns exhibited by the composite plate under various loading conditions. This investigation sheds light on how the combination of ply angles influences the overall dynamic behavior of the laminated structure, particularly in the presence of the surface-bonded piezo-patches.

Understanding the variation in mode shapes for different lamination arrays is crucial for tailoring the structural design to achieve specific performance objectives. Moreover, this analysis aids in identifying modes that may be more sensitive to changes in ply angles, allowing researchers to optimize the laminate configuration to meet targeted vibration and energy harvesting requirements.

Table 3.3: First six mode shapes for the different four ply angles

Mode Shapes	**Lamination Sequences**			
	0/0/0/0	45/45/45/45	90/90/90/90	-45/45/45/-45
First Mode Shape	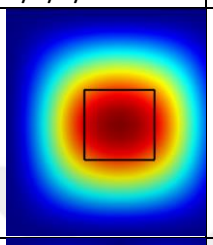	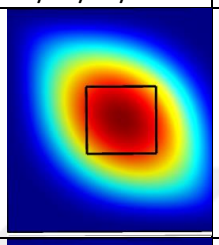	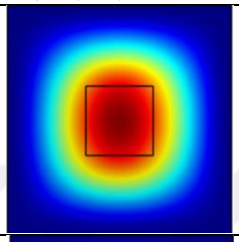	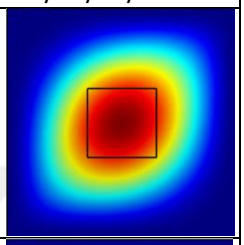
Second Mode Shape	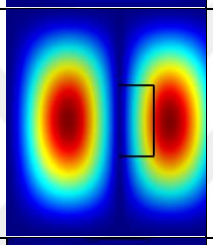	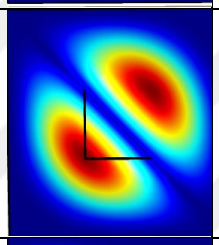	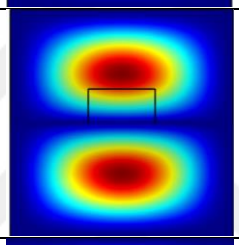	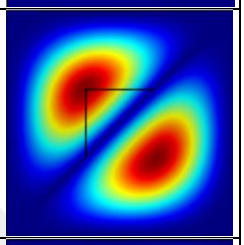
Third Mode Shape	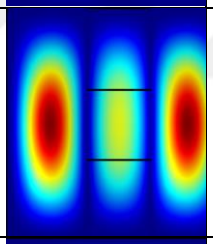	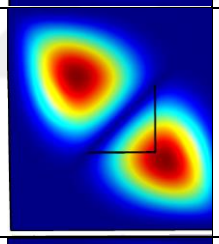	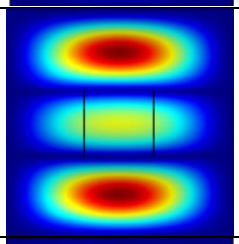	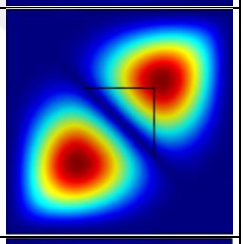
Fourth Mode Shape	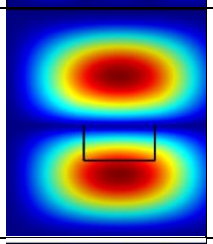	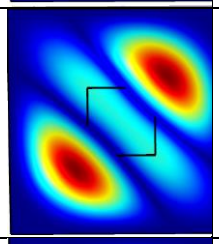	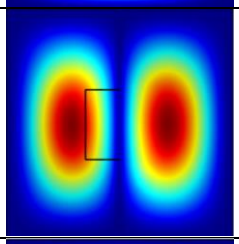	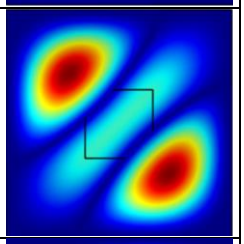
Fifth Mode Shape	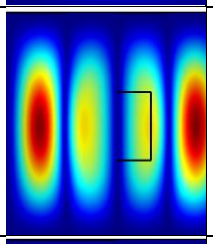	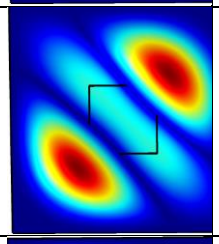	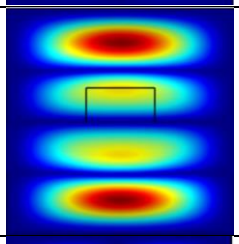	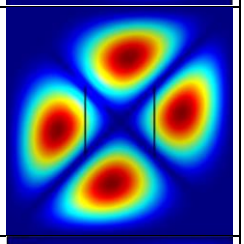
Sixth Mode Shape	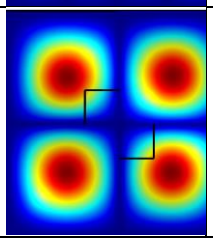	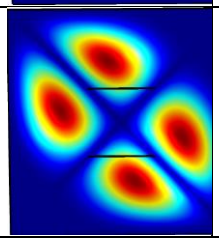	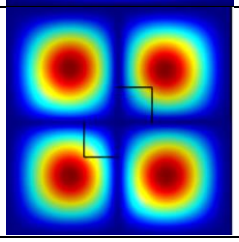	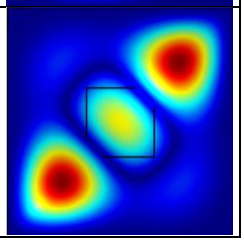

3.3. Harmonic Analysis for Displacement FRFs and Voltage FRFs

The frequency response function (FRF) analysis for both input displacement-to-force and voltage-to-force is performed to comprehensively study the dynamic behavior of the primary composite structure integrated with surface-bonded piezo-patches. To initiate the analysis, a transverse point force of 1 N is applied at the upper section of the structure, precisely at position coordinates of (125) mm. The resulting vibrations are then recorded at coordinates of (375) mm. These measurements serve as critical data points for assessing the system's response to external loading conditions and its dynamic characteristics.

The displacement FRFs are subsequently obtained and graphically presented for four different lamination sequences in Figure 3.1.: $[0/0]_s$, $[90/90]_s$, $[45/\text{-}45]_s$, and $[0/\pm45/90]_s$. These lamination sequences correspond to various combinations of ply orientations within the composite plate, and their influence on the frequency response is carefully analyzed. To ensure robustness and accuracy, the analysis is conducted for ten distinct vibration modes, employing both analytical and finite element analysis solutions. This thorough examination facilitates a comprehensive understanding of the composite plate's dynamic behavior under different loading scenarios and the effect of lamination sequences on its vibrational response.

To acquire the voltage FRFs or frequency response functions for voltage-to-force input, the voltage output across the resistive load is measured. In both the analytical model and finite element modeling, a resistance value of $10^6\ \Omega$ is utilized to closely approximate an open circuit condition. The voltage FRFs for ten distinct modes are then presented graphically in Figure 3.1., considering four different lamination sequences: $[0/0]_s$, $[90/90]_s$, $[45/\text{-}45]_s$, and $[0/\pm45/90]_s$. The graphs illustrate the relationship between the applied voltage and the resulting force response, providing valuable insights into the system's electrical behavior under various loading conditions.

All graphs have two y-axes, each representing a distinct aspect of the response. The y-axis on the left corresponds to the voltage FRF, demonstrating the voltage output

across the resistive load in response to the applied force excitation. On the other hand, the y-axis on the right portrays the displacement FRF, illustrating the structural response in terms of displacements in different vibration modes. This dual representation allows for a comprehensive understanding of the complex interplay between electrical and mechanical behaviors in the composite plate with surface-bonded piezo-patches.

By conducting thorough frequency response function analysis for both input displacement-to-force and voltage-to-force, engineers gain essential insights into the system's dynamic characteristics, enabling them to optimize the structural design and enhance the efficiency of energy harvesting using piezo-patches. The comprehensive data obtained from the analytical model and finite element analysis allow for precise comparisons, ensuring the accuracy and reliability of the proposed analytical approach for simulating the complex behavior of the composite structure under various excitation conditions.

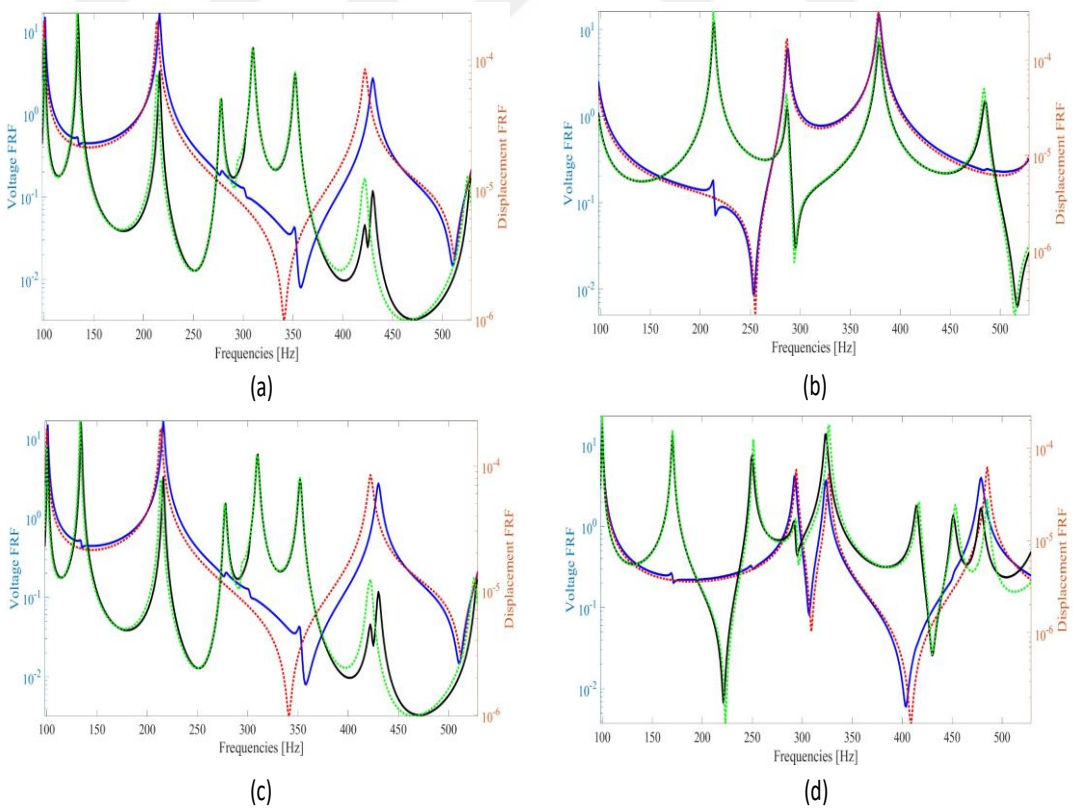

Figure 3.1: Displacement and voltage FRF of system for different lamination sequences: (a) $[0,0]_s$, (b) $[45, -45]_s$, (c) $[90,90]_s$, (d) $[0/\pm45/90]_s$.

3.4. Power Outputs

Within this section, we explore the maximum power outputs and average power output values of a composite plate with dimensions of 50x50 cm, integrated with piezo patches of 150x150 mm and 1 N point load is applied at corner. The plate is configured with various lamination sequences, including $[0/0]_s$, $[90/90]_s$, $[45/-45]_s$, and $[0/\pm45/90]_s$. The calculations are conducted using Equation (78) and Equation (79), which provide valuable insights into the energy harvesting potential of the system.

The obtained values are presented in Table 3.4, with the first column displaying the V_1 and V_3 values, which are vital parameters characterizing the lamination configurations within the composite plate. The second column showcases the corresponding maximum power output values, which represent the peak energy generation achievable under specific lamination sequences. The third column illustrates the average value of the power output, reflecting the overall energy harvesting efficiency of each configuration.

Table 3.4: Power output of cases of $[0/0]_s$, $[45/-45]_s$, $[0/\pm45/90]_s$ and $[90/90]_s$.

$[V_1\ V3]$	Maximum Power Output (mW)	Averages of Power Output (mW)
[1 1]	2872,93	547,52
[0 -1]	4018,29	675,35
[0 0]	3970,82	667,78
[-1 1]	2872,93	547,52

3.5. Optimization Results

This section focuses on the power outputs and average power outputs achieved through optimization for four laminated composite plates of varying sizes, each integrated with a 150x150 mm piezoelectric patch.

Figure 3.2. illustrates the x and y axes, along with the specific points of application ($x_{i,1}$ and $y_{i,1}$) and measurement ($x_{i,2}$ and $y_{i,2}$) for each case. The investigation commences with a 500x500 mm composite plate, where a transverse load of 1 N is applied at coordinates $x_{i,1}$=125 mm and $y_{i,1}$=125 mm on both the x and y axes. The resulting power outputs are measured at coordinates $x_{i,2}$=375 mm and $y_{i,2}$=375 mm. Fig. 3.2 (I). shows the position of the load. Additionally, a force of 1 N is applied to the same-sized composite plate at position coordinates $x_{i,1}$=250 mm and $y_{i,1}$=125 mm, and measurements are taken at $x_{i,2}$=375 mm and $y_{i,2}$=375 mm. Also Fig. 3.2.(II). shows the position of the load.

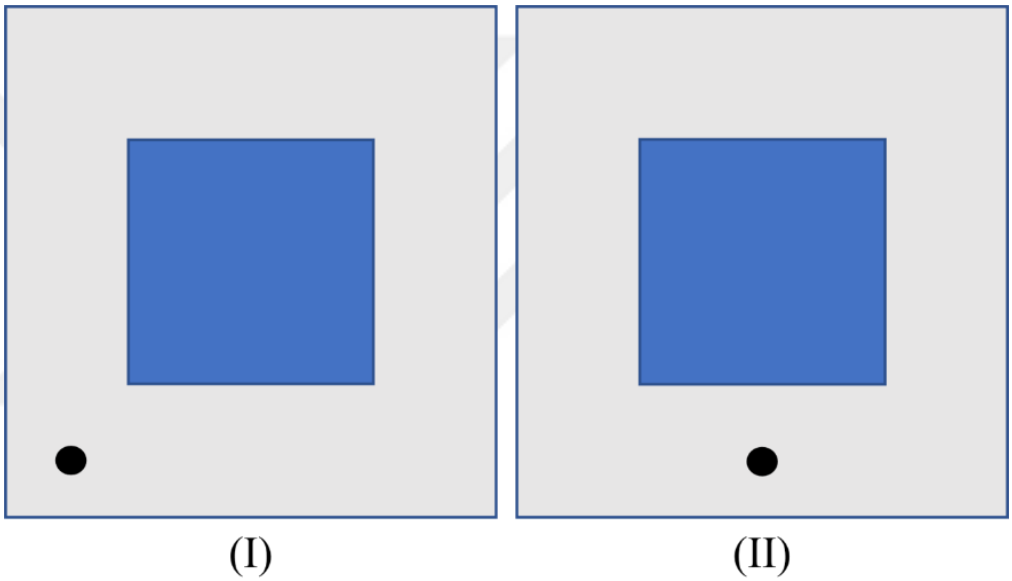

Figure 3.2: Representation of the position of the forces: (I) Force in the corner, (II) Force in the middle.

To represent the design space and outcomes effectively, Miki's diagram is utilized. The subsequent Figure 3.3 contains comprehensive information on the maximum power outputs and average power outputs for these cases. By considering different lamination parameters (V_1 and V_3), optimal power output configurations are determined for the various load application points.

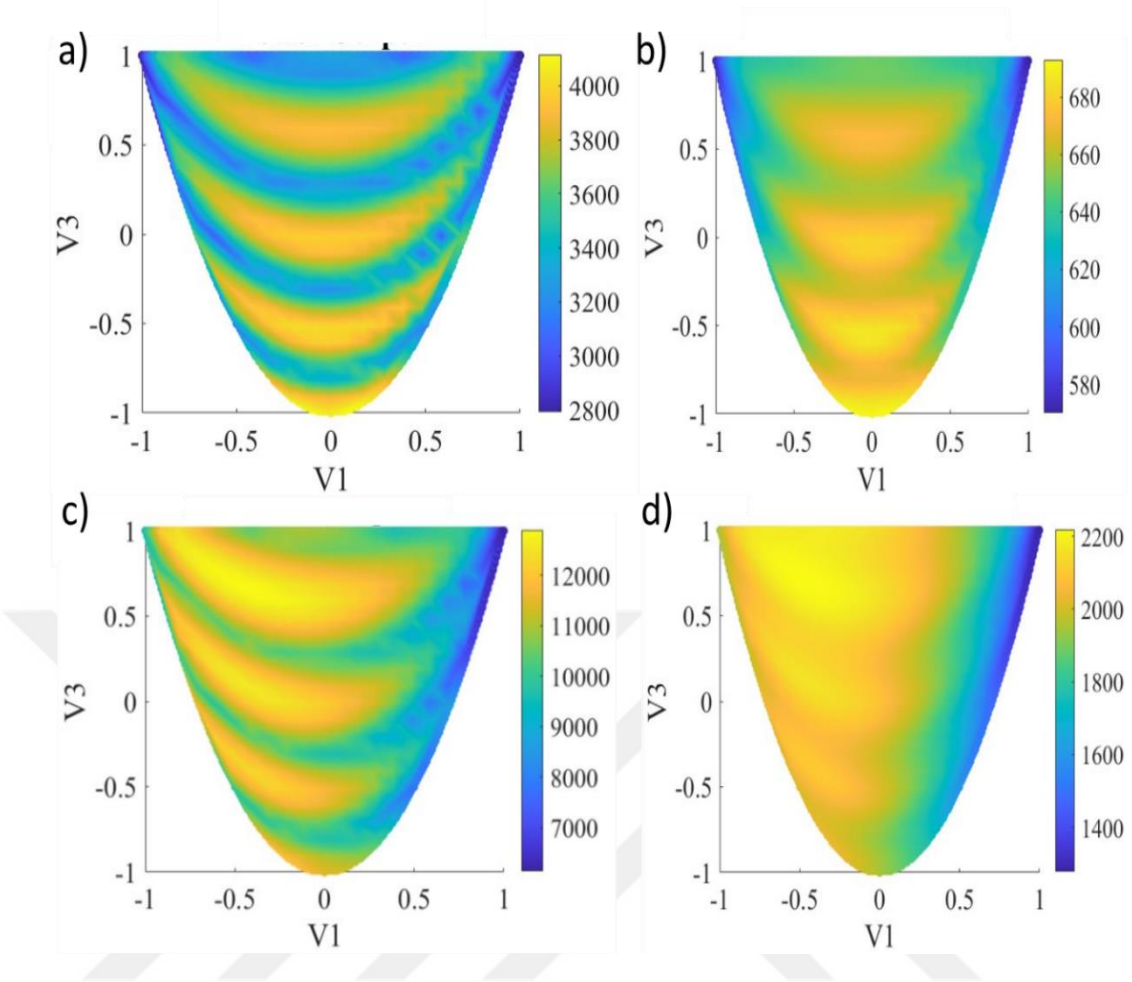

Figure 3.3: a) Maximum power out in case of force in the corner (I), (b) average of power output in case of force in the corner (I), c) maximum power out in case of force in the center (II), (d) average of power output in case of force in the center (II).

Table 3.5 displays the variations in maximum power output and average power output for two different scenarios. It's evident that altering the force location affects both maximum and average power outputs. Notably, the enhancement in maximum power output exceeds the improvement in average power output within the frequency range. It's possible to achieve up to a 48% improvement by adjusting lamination parameters, leading to a significant boost in power output.

Table 3.5: Comparison of maximum and average maximum power output with unidirectional case.

Loading location	$P_{out_{max}}$ Unidirectional [mW]	$P_{out_{max}}$ [mW]	Difference (%)	$P_{out_{average}}$ Unidirectional [mW]	$P_{out_{average}}$ [mW]	Difference (%)
Center	8675.25	12913.7	48.83	1645.2	2182.01	32.64
Corner	3060.85	4028.11	31.34	598.02	675.35	13.01

After optimizing based on these parameters, the best results for maximum power output are achieved with $V_1 = -0.4, V_3 = 0.7$ when using a 50×50 cm composite plate with the load placed in the middle of the bottom edge. However, for a composite plate of the same size with the load at the corner, the optimum values for maximum power output are $V_1 = 0.2, V_3 = -0.9$.

4. CONCLUSIONS

The research investigation conducted in this study has yielded compelling evidence that the careful selection of appropriate lamination parameters holds the potential to significantly enhance the maximum power output of composite plates. This discovery is of immense significance, as it paves the way for optimizing the design of composite plates across various industries, including aerospace and renewable energy systems. To initiate the study, the researchers focused on determining the natural frequencies of composite plates with distinct lamination parameters. Through meticulous harmonic analyses, valuable insights were gained into the dynamic behavior of these plates under different conditions.

To ensure the robustness and accuracy of the findings, thorough validation was conducted using COMSOL, a renowned commercial finite element analysis software known for its reliability. With validated results in hand, the researchers proceeded to evaluate the maximum power outputs and average values of power outputs across a comprehensive range of lamination parameters and composite materials. This assessment encompassed a diverse array of plate cases, allowing for a thorough exploration of various configurations.

The optimization process based on varying lamination parameters thoroughly examined the power output values of composite plates subjected to force at different points. Remarkably, the maximum power output was achieved under specific lamination parameter combinations. For instance, in the case of a 50x50 cm composite plate with a load applied at its center, the optimal lamination parameter values were found to be $V_1 = -0.4$ and $V_3 = 0.7$. Conversely, when the load was positioned at the corner of a composite plate of the same dimensions, the maximum power output was obtained at parameter values $V_1 = 0.2$ and $V_3 = -0.9$.

The optimization process revealed specific combinations of V_1 and V_3 that unlock the full potential of energy harvesting capabilities in each plate configuration.

The comprehensive and meticulous analysis conducted in this research has yielded a wealth of extensive data, providing valuable insights and robust evidence that underscore the significant influence of carefully selected lamination parameters on the power output maximization of composite plates across different cases Such profound revelations hold far-reaching practical implications that can revolutionize critical applications in the aerospace industry.

The optimized design of composite plates has the potential to elevate overall performance and efficiency, contributing to advancements in aircraft structures, leading to lighter and more fuel-efficient aircraft, and potentially reducing carbon emissions. Additionally, the findings from this study are of paramount importance in advancing renewable energy systems, where the pursuit of greater energy generation and sustainability is at the forefront of global endeavors.

REFERENCES

Abdalla, M. M., Setoodeh, S., & Gürdal, Z. (2007). Design of variable stiffness composite panels for maximum fundamental frequency using lamination parameters. *Composite Structures*, *81*(2), 283–291. https://doi.org/10.1016/j.compstruct.2006.08.018.

Aridogan, U., Basdogan, I., & Erturk, A. (2014). Multiple patch–based broadband piezoelectric energy harvesting on plate-based structures. *Journal of Intelligent Material Systems and Structures*, *25*(14), 1664–1680. https://doi.org/10.1177/1045389X14544152.

Assaee, H., & Hasani, H. (2015). Forced vibration analysis of composite cylindrical shells using spline finite strip method. *Thin-Walled Structures*, *97*, 207–214. https://doi.org/10.1016/j.tws.2015.09.014.

Bardell, N. S., Dunsdon, J. M., & Langley, R. S. (1997). Free and forced vibration analysis of thin, laminated, cylindrically curved panels. *Composite Structures*, *38*(1–4), 453–462. https://doi.org/10.1016/S0263-8223(97)00080-9.

Bhat, R. B. (1985). Natural frequencies of rectangular plates using characteristic orthogonal polynomials in rayleigh-ritz method. *Journal of Sound and Vibration*, *102*(4), 493–499. https://doi.org/10.1016/S0022-460X(85)80109-7

Corrêa de Godoy, T., & Areias Trindade, M. (2011). Modeling and analysis of laminate composite plates with embedded active–passive piezoelectric networks. *Journal of Sound and Vibration*, *330*(2), 194–216. https://doi.org/10.1016/j.jsv.2010.08.010.

Covaci, C., & Gontean, A. (2020). Piezoelectric Energy Harvesting Solutions: A Review. *Sensors*, *20*(12), Article 12. https://doi.org/10.3390/s20123512.

Detwiler, D. T., Shen, M.-H. H., & Venkayya, V. B. (1995). Finite element analysis of laminated composite structures containing distributed piezoelectric actuators and sensors. *Finite Elements in Analysis and Design*, *20*(2), 87–100. https://doi.org/10.1016/0168-874X(95)00013-J.

Duan, W. H., Wang, Q., & Quek, S. T. (2010). Applications of Piezoelectric Materials in Structural Health Monitoring and Repair: Selected Research Examples. *Materials*, *3*(12), 5169–5194. https://doi.org/10.3390/ma3125169.

Erturk, A., & Inman, D. J. (2009). An experimentally validated bimorph cantilever model for piezoelectric energy harvesting from base excitations. *Smart Materials and Structures*, *18*(2), 025009.

Fleming, A. J., & Moheimani, S. O. R. (n.d.). *Adaptive piezoelectric shunt damping*.

Ghazanfarian, J., Mohammadi, M. M., & Uchino, K. (2021). Piezoelectric Energy Harvesting: A Systematic Review of Reviews. *Actuators*, *10*(12), 312. https://doi.org/10.3390/act10120312.

Gohari, S., Sharifi, S., & Vrcelj, Z. (2016). New explicit solution for static shape control of smart laminated cantilever piezo-composite-hybrid plates/beams under thermo-electro-mechanical loads using piezoelectric actuators. *Composite Structures*, *145*, 89–112. https://doi.org/10.1016/j.compstruct.2016.02.047.

Gozum, M. M., Aghakhani, A., Serhat, G., & Basdogan, I. (2018). Electroelastic modeling of thin-laminated composite plates with surface-bonded piezo-patches using Rayleigh–Ritz method. *Journal of Intelligent Material Systems and Structures*, *29*(10), 2192–2205. https://doi.org/10.1177/1045389X18758189.

Han, X., Neubauer, M., & Wallaschek, J. (2013). Improved piezoelectric switch shunt damping technique using negative capacitance. *Journal of Sound and Vibration*, *332*(1), 7–16. https://doi.org/10.1016/j.jsv.2012.08.001.

Honda, S., Narita, Y., & Sasaki, K. (2009). Discrete Optimization for Vibration Design of Composite Plates by Using Lamination Parameters. *Advanced Composite Materials*, *18*(4), 297–314. https://doi.org/10.1163/156855109X434739.

IEEE Standard on Piezoelectricity. (n.d.). IEEE. https://doi.org/10.1109/IEEESTD.1988.79638.

Ju, M., Dou, Z., Li, J.-W., Qiu, X., Shen, B., Zhang, D., Yao, F.-Z., Gong, W., & Wang, K. (2023). Piezoelectric Materials and Sensors for Structural Health Monitoring: Fundamental Aspects, Current Status, and Future Perspectives. *Sensors*, *23*(1), 543. https://doi.org/10.3390/s23010543

Khetre, S. N., Nitnaware, P. T., & Meshram, A. M. (n.d.). Design and Analysis of Composite High Pressure Vessel with Different Layers using FEA. *International Journal of Engineering Research*, *3*(11).

Kim, H. S., Kim, J.-H., & Kim, J. (2011). A review of piezoelectric energy harvesting based on vibration. *International Journal of Precision Engineering and Manufacturing*, *12*(6), 1129–1141.

Lahe, P., Basdogan, I., & Aghakhani, A. (2018). Passive vibration control of a plate via piezoelectric shunt damping with FEM and ECM. In T. E. Matikas (Ed.), *Smart Materials and Nondestructive Evaluation for Energy Systems IV* (p. 2). SPIE. https://doi.org/10.1117/12.2295703.

Li, T., & Lee, P. S. (2022). Piezoelectric Energy Harvesting Technology: From Materials, Structures, to Applications. *Small Structures*, *3*(3), 2100128. https://doi.org/10.1002/sstr.202100128.

Meirovitch, L. (2001). *Fundamentals of vibrations*. McGraw-Hill.

Miki, M. (1985). *Design of laminated fibrous composite plates with required flexural stiffness*. ASTM International West Conshohocken, PA.

Motlagh, P. L., Anamagh, M. R., Bediz, B., & Basdogan, I. (2021). Electromechanical analysis of functionally graded panels with surface-integrated piezo-patches for optimal energy harvesting. *Composite Structures*, *263*, 113714. https://doi.org/10.1016/j.compstruct.2021.113714.

Motlagh, P. L., Bediz, B., & Basdogan, I. (2020). A spectral Tchebychev solution for electromechanical analysis of thin curved panels with multiple integrated piezo-patches. *Journal of Sound and Vibration*, *486*, 115612. https://doi.org/10.1016/j.jsv.2020.115612.

Park, J. H., Hwang, J. H., Lee, C. S., & Hwang, W. (2001). Stacking sequence design of composite laminates for maximum strength using genetic algorithms. *Composite Structures*, *52*(2), 217–231. https://doi.org/10.1016/S0263-8223(00)00170-7.

Priya, S., Song, H.-C., Zhou, Y., Varghese, R., Chopra, A., Kim, S.-G., Kanno, I., Wu, L., Ha, D. S., Ryu, J., & Polcawich, R. G. (2019). A Review on Piezoelectric Energy Harvesting: Materials, Methods, and Circuits. *Energy Harvesting and Systems*, *4*(1), 3–39. https://doi.org/10.1515/ehs-2016-0028.
Qing, X., Li, W., Wang, Y., & Sun, H. (2019). Piezoelectric Transducer-Based Structural Health Monitoring for Aircraft Applications. *Sensors*, *19*(3), 545. https://doi.org/10.3390/s19030545.

Rao, S. S. (2007). *Vibration of continuous systems*. Wiley.

Sezer, N., & Koç, M. (2021). A comprehensive review on the state-of-the-art of piezoelectric energy harvesting. *Nano Energy*, *80*, 105567. https://doi.org/10.1016/j.nanoen.2020.105567.

Torres, E. O., & Rincon-Mora, G. A. (2009). Electrostatic Energy-Harvesting and Battery-Charging CMOS System Prototype. *IEEE Transactions on Circuits and Systems I: Regular Papers*, *56*(9), 1938–1948. https://doi.org/10.1109/TCSI.2008.2011578.

Trias, D., Maimí, P., & Blanco, N. (2016). Maximization of the fundamental frequency of plates and cylinders. *Composite Structures*, *156*, 375–384. https://doi.org/10.1016/j.compstruct.2015.08.034.

Tsai, S. W., & Hahn, T. (n.d.). *INTRODUCTION TO COMPOSITE MATERIALS*.

Wan, X., Cong, H., Jiang, G., Liang, X., Liu, L., & He, H. (2023). A Review on PVDF Nanofibers in Textiles for Flexible Piezoelectric Sensors. *ACS Applied Nano Materials*, *6*(3), 1522–1540. https://doi.org/10.1021/acsanm.2c04916.

Yan, B., Wang, K., Hu, Z., Wu, C., & Zhang, X. (2017). Shunt Damping Vibration Control Technology: A Review. *Applied Sciences*, *7*(5), 494. https://doi.org/10.3390/app7050494.

Yang, B., Lee, C., Xiang, W., Xie, J., Han He, J., Kotlanka, R. K., Low, S. P., & Feng, H. (2009). Electromagnetic energy harvesting from vibrations of multiple frequencies. *Journal of Micromechanics and Microengineering*, *19*(3), 035001. https://doi.org/10.1088/0960-1317/19/3/035001.

Yoon, H., Youn, B. D., & Kim, H. S. (2016). Kirchhoff plate theory-based electromechanically-coupled analytical model considering inertia and stiffness effects of a surface-bonded piezoelectric patch. *Smart Materials and Structures*, *25*(2), 025017. https://doi.org/10.1088/0964-1726/25/2/025017.

Zhou, M., Al-Furjan, M. S. H., & Wang, B. (2018). Modeling and Efficiency Analysis of a Piezoelectric Energy Harvester Based on the Flow Induced Vibration of a Piezoelectric Composite Pipe. *Sensors*, *18*(12), Article 12. https://doi.org/10.3390/s18124277.

BIOGRAPHY

Mustafa Kemal ACAR is a research and teaching assistant at Gebze Technical University. He obtained his bachelor's from Konya Teknik University in 2020. He is doing his master's at the Mechanical Engineering Department under the supervision of Dr. Peyman Lahe Motlagh about smart composites to achieve high power output from energy harvesting concepts.

PUBLICATIONS AND PRESENTATIONS FROM THE THESIS

Acar M.K., Motlagh P.L., (2023), "A new framework for optimizing energy harvesting from smart composites integrated with piezoelectric patches utilizing lamination parameters", Engineering Solid Mechanics, DOI: 10.5267/j.esm.2023.10.003.

Acar M.K., Motlagh P.L., (2023), "Optimization of Power Output in Smart Composite Panel Integrated with Piezoelectric Patches", 12th Ankara International Aerospace Conference (AIAC), AIAC-2023-047, Ankara, Turkey, 13-15 September.